Royal Netherlands Institute for Sea Research

Liang, J.; Richter, N.; Xie, H.; Zhao, B.; Si, G.; Wang, J.; Hou, J.; Zhang, G.; Russell, J.M. (2023). Branched glycerol dialkyl glycerol tetraether (brGDGT) distributions influenced by bacterial community composition in various vegetation soils on the Tibetan Plateau. *Palaeogeogr. Palaeoclimatol. Palaeoecol. 611*: 111358. DOI : 10.1016/j.palaeo.2022.111358

Published version: https://dx.doi.org/10.1016/j.palaeo.2022.111358

NIOZ Repository: http://imis.nioz.nl/imis.php?module=ref&refid=361053

[Article begins on next page]

Branched glycerol dialkyl glycerol tetraether (brGDGT) distributions influenced by bacterial community composition in various vegetation soils on the Tibetan Plateau

Jie Liang [1,2], Nora Richter[3], Haichao Xie [1], Boyang Zhao[2], Guicai Si[4], Jian Wang[5], Juzhi Hou[1*], Gengxin Zhang [1*], James M. Russell [2]

1. State Key Laboratory of Tibetan Plateau Earth System, Environment and Resources (TPESER), Institute of Tibetan Plateau Research, Chinese Academy of Sciences, Beijing 100101, China
2. Department of Earth, Environmental, and Planetary Sciences, Brown University, Providence 02912, USA
3. NIOZ Royal Institute for Sea Research, Department of Marine Microbiology and Biogeochemistry, P.O. Box 59, 1790 AB Den Burg, Texel, The Netherlands
4. Lanzhou Center for Oil and Gas Resources, Institute of Geology and Geophysics, Chinese Academy of Sciences, Lanzhou, 730000, China
5. Land and Resource College, China West Normal University, Nanchong, Sichuan, 637002, China

* Corresponding author:

Gengxin Zhang, zhangg@itpcas.ac.cn

Juzhi Hou, houjz@itpcas.ac.cn

Abstract

Branched glycerol dialkyl glycerol tetraether (brGDGT) lipids are membrane-spanning lipids of some bacteria that are sensitive to environmental gradients, which makes it possible to use brGDGT proxies to estimate changes in environmental temperatures in paleoenvironmental studies. However, it is currently unknown whether the observed correlations of temperature and brGDGT distribution in natural samples are driven by directly changing bacterial membrane fluidity and permeability, or by a shift in the bacterial community. Here we present brGDGT distributions along an elevation gradient (704–3760 m) in the southeastern Tibetan Plateau, spanning gradients in temperature and vegetation. Analysis of brGDGTs shows that their distributions are significantly influenced by vegetation-intermediated soil temperature, in addition to mean annual air temperature, soil pH, and other environmental variables. Different vegetation types contribute to soil temperature and bacterial community changes. Consequently, these different groups of bacteria result in changes in the relative abundance of brGDGTs. Our results show that temperature and pH indirectly influence cyclopentane-containing brGDGTs via changes in the bacterial community. Genetic analyses reveal that in addition to Acidobacteria, Proteobacteria, Nitrospira, Bacteroidetes, Actinobacteria, and Verrucomicrobia could be potential candidates as brGDGT producers. These results indicate that changes in the vegetation and bacterial community should be taken into consideration when applying brGDGT proxies to reconstruct past changes in climate.

Keywords: vegetation; soil brGDGTs; MBT′; Tibetan Plateau; paleoclimate; bacterial community

1. Introduction

Branched glycerol dialkyl glycerol tetraethers (brGDGTs) are membrane-spanning lipids that are ubiquitous in the nature world (Raberg et al., 2022), including soils (Wang and Liu, 2021; Weijers et al., 2007; Yang et al., 2014a), lakes (Dang et al., 2018; Russell et al., 2018; Zhao et al., 2021), as well as loess and peat bogs (Naafs et al., 2017b; Wang et al., 2020). BrGDGT distributions correlate with mean annual air temperatures (hereafter MAAT) or growing season temperatures and pH leading to the development of both local and global empirical calibrations for different environmental settings (Crampton-Flood et al., 2020; De Jonge et al., 2014; Naafs et al., 2017a; Peterse et al., 2012). This has led to the application of quantitative brGDGT reconstructions to continental paleoclimate records spanning the Holocene (Wang et al., 2021) and longer geologic timescales (Crampton-Flood et al., 2021; Inglis et al., 2017).

Previously, the distributions of brGDGTs were analyzed by high-performance liquid chromatography–mass spectrometry (HPLC–MS) using one Prevail Cyano column (here termed the “old method”). Improved chromatographic techniques using four Alltima silica columns allowed for the separation and quantification of 5- and 6-methyl brGDGTs (De Jonge et al., 2014; Hopmans et al., 2016; hearafter termed "new method"), a hybrid 5/6-methyl isomer (Weber et al., 2015) and H-shaped brGDGTs (Baxter et al., 2019; Naafs et al., 2018; Tang et al., 2021). Evaluation of the global soil dataset found that the relative abundance of 6-methyl brGDGTs was influenced predominantly by pH (De Jonge et al., 2014). Although the latest brGDGT-MAAT calibrations excluding 6-methyl brGDGT have improved the correlation coefficient (R^2) and root mean square error (RMSE), there is still a large warm bias in the

calibration when applied to specific regions (Chen et al., 2021; Wang and Liu, 2021). This suggests other natural (e.g., vegetation, soil type, and water content) and human factors (e.g., agriculture and management) may affect soil brGDGT abundances and therefore temperature calibrations. For example, Liang et al. (2019) found that brGDGT distributions in vegetated soil are sensitive to MAAT, whereas brGDGTs in bare soil are mainly controlled by water content. It is well known that vegetation change is critical component to modeling Holocene temperature evolution (Thompson et al., 2022), however, we have a limited understanding of how changes in vegetation may affect the brGDGT-paleothermometer.

It is increasingly recognized that changes in the source organism community can directly influence these biomarker composition (De Jonge et al., 2021; De Jonge et al., 2019; Liao et al., 2021). However, most producers of brGDGTs have not been identified, hampering our understanding of how brGDGT production varies with environmental changes. Analyses of brGDGTs in Dutch peat bogs and subsequent culture experiments suggest that brGDGTs are synthesized by heterotrophic bacteria of the phylum Acidobacteria (Sinninghe Damsté et al., 2018; Sinninghe Damsté et al., 2014; Sinninghe Damsté et al., 2011). Although these are the only known brGDGT-producers, other studies suggest that a broader range of microorganisms are involved in brGDGT production (De Jonge et al., 2019; Sinninghe Damsté et al., 2018).

The major challenges limiting the application of brGDGT proxies to paleorecords are (1) the complex and wide-range of environmental parameters influencing soil brGDGT distributions (e.g. seasonality, water availability and vegetation); (2) soil reconstructed temperature related to different environmental temperature (in situ soil temperature vs air temperature); (3) lack of knowledge of

brGDGT-producing microbial community or a physiological response by certain bacteria. Here, we present investigations of surface soil samples with very distinct vegetation zones across fourteen elevational gradients ranging from 704 to 3760 m on the south Tibetan Plateau. We analyzed both brGDGT composition and bacterial community composition to examine the influence of vegetation, soil pH, and temperature on the distributions of bacterial communities and brGDGT compounds. Our main objectives are to evaluate the potential effects of vegetation on brGDGT distributions, how altitudinal differences impact the temperature bias recorded in our brGDGT proxy, and identifying potential brGDGT-producers.

2. Materials and Methods

2.1 Site description and sample collection

Soil samples were collected on Galongla Mountain in Motuo County, Southeast Tibetan Plateau, China (27°36'–29°50' N, 93°42'–96°36' E; Fig. 1a). There are six vegetation zones along the mountain: tropical rainforest (TRF; 600–1100 m), evergreen broad-leaved forest (EBF; 1100–2000 m), evergreen/semi-evergreen broad-leaved forest (SEBF; 2000–2500 m), temperate mixed coniferous broad-leaved forest (TCF; 2500–3000 m), frigid-temperate coniferous forest (FCF; 2500–3000 m), and frigid-temperate coniferous forest and frigid shrub meadow (FSM; 3700–4000 m) (Fig. 1b; Table 1). Soil samples were collected at 14 sites from 704 to 3760 m above sea level across the vegetation zones. At each site, 10 soil samples were randomly collected within a quadrant (10 m by 10 m in the forests and 5 m by 5 m in the shrublands and/or grasslands), for a total of 134 samples. Five hundred grams of soil

was collected for each sample after the removal of plant fragments, from which a 50 g subsample was stored at -80 °C prior to DNA and lipid analysis.

2.2 Environmental variables

Monthly temperature and precipitation at each site were obtained from the Worldclim2 dataset (https://www.worldclim.org/data/). The Worldclim2 dataset interpolates monthly temperature data compiled from globally distributed weather stations to a 30 arc-second spatial resolution across a temporal range from 1970–2000 (Fick and Hijmans, 2017). The mean annual soil temperatures were gained from global gridded soil temperature maps according to Lembrechts et al. (2022), which used over 8500 time series of soil temperatures measured in situ across the world and a machine learning approach to model predictor variables of the soil and air temperature offset, and finally interpolate soil temperatures (Lembrechts et al., 2022). We validated this soil temperature dataset in China by comparing the gridded soil temperature with mean annual soil temperatures that were monitored using temperature loggers (Thermochron iButton ®DS1922L-F5#) (Wang et al., 2020). We found that the gridded soil temperature and measured soil temperatures have a significant positive correlation ($R = 0.98$, $p < 0.001$; Fig. S1), suggesting that the global gridded soil temperature maps can be used in this study. Soil water content was determined by drying soil samples at 105 °C for 12 h. pH was determined after hydrating the soil to a soil to water ratio of 1:2.5 (v/v) according to Weijers et al. (2007). The soil conductivity was obtained by measuring the supernatants with a conductivity meter. Soil (clay/sand/silt percentage) was digested with H_2O_2, followed by the determination of the soil particle distribution with a Microtrac S3500 analyzer.

Total nitrogen (TN) was determined using a modified Kjeldahl method (Bremner, 1960). Total organic carbon (TOC) was measured with air-dried solid soil using a TOC analyzer (TOC-VCPH, Shimadzu, Japan). Total phosphorus (TP) was determined using the molybdenum blue method (Dick and Tabatabai, 1977).

2.3 brGDGT analysis

Freeze-dried samples (5–6 g) were extracted ultrasonically with dichloromethane/methanol (9:1, v/v) (15 min × 3, 30 °C) to extract soluble lipids. Activated alumina was used as a stationary phase for separating brGDGTs, and the non-polar and polar fractions (the latter containing brGDGTs) were eluted using *n*-hexane/dichloromethane (9:1, v/v) and dichloromethane/methanol (1:1, v/v), respectively. After blowing down the polar fraction with N_2, the sample was dissolved in *n*-hexane/isopropanol (99:1, v/v), and a 0.45 μm PTFE filter was used to remove particulate matter prior to HPLC–MS analysis.

BrGDGT analysis was performed using an ultra high-performance liquid chromatograph (Waters ACQUITY UHPLC I-Class/Xevo TQD) with atmospheric pressure chemical ionization coupled to a triple quadrupole mass spectrometer (UHPLC–APCI–MS). BrGDGTs were separated over an Alltech Prevail Cyano column (150 mm × 2.1 mm, 3 μm). The instrumental setup for the UHPLC was as follows: column temperature 40 °C, injection volume 5 μL, and flow rate 0.3 mL/min. For the mobile phase *n*-hexane and *n*-hexane/isopropanol (9:1, v/v) were used, and the elution procedure followed Yang et al. (2014b). The analysis was performed in Single Ion Monitoring (SIM) mode via $[M+H]^+$ of brGDGTs (1050, 1048, 1046, 1036, 1034, 1032, 1022, 1020, 1018). The definition of the structure and number of brGDGTs

follows Peterse et al. (2012). All brGDGTs were displayed as fractional abundances.

The cyclization index of branched tetraethers (CBT), methylation index of branched tetraethers (MBT′) and reconstructed mean annual air temperature (MAATre) were calculated as previously defined (Peterse et al., 2012).

$$CBT = -log\left(\frac{Ib+IIb}{Ia+IIa}\right) \quad (1)$$

$$MBT' = \frac{Ia+Ib+Ic}{Ia+Ib+Ic+IIa+IIb+IIc+IIIa} \quad (2)$$

$$MAATre = 0.81 - 5.67 \times CBT + 31.00 \times MBT' \quad (3)$$

2.4 Bacterial community analysis

DNA was extracted from all samples (0.5 g of fresh soil samples) following the method described by Hu et al. (2020). DNA quality was assessed using a Nanodrop ND-2000c UV–Vis spectrophotometer. PCR amplification of the 16S rRNA gene hypervariable region V4 was performed with the primers 515F and 806R (515F: 5'-GTGCCAGCMGCCGCGGTAA-3'); 806R: 5'-GGACTACHVGGGTWTCTAAT-3'). The 2×250 bp paired-end sequencing of PCR amplicons targeting V4 hypervariable regions of the 16S rRNA gene was conducted on a MiSeq platform (Illumina, San Diego, CA) at the Institute for Environmental Genomics, University of Oklahoma. The preprocessing of the Illumina sequencing data and the downstream analysis, including taxonomic assignment and diversity analysis, were performed using QIIME (v. 1.8.0; Caporaso et al., 2010) and an in-house Galaxy software platform (IEG sequence analysis pipeline, http://zhoulab5.rccc.ou.edu). All raw sequences were first separated into samples via sample-specific barcodes. In the Galaxy analysis pipeline, chimeras were removed using UCHIME (Edgar et al., 2011), chimera-free sequences

were clustered to generate operational taxonomic units (OTUs) with a cutoff value of 97% sequence identity using UPARSE (version usearchV7.0.1001_i86linux64) (Edgar, 2013), and the final OTU table was further rarefied with an even-sequencing depth of 13,000. Taxonomic classification was performed in Galaxy with the RDP Classifier (Cole et al., 2009).

2.5 Statistics analysis

All statistical analyses were performed using R statistical software (version 4.0.5; R Core Team, 2021). To assess the relationship between vegetation types and brGDGT fractional abundances, we performed indirect principal component analysis (PCA) using the *FactoMineR* package (Husson et al., 2016) and a heatmap with the clustering method performed by the *ComplexHeatmap* package (Gu et al., 2016). A heatmap cluster was generated using z score transformation of brGDGT relative abundance. PCA analyses of the fractional abundance of brGDGTs were performed on centered and standardized abundances. We performed redundancy analysis (RDA) by *vegan* package (Oksanen et al., 2020) to assess the relationship between environmental variables (MAAT, MAF, Tsoil, pH, conductivity, water content, bacterial community, relative content of sand, clay and sand, TOC, TN and TP).

Analysis of similarity (ANOSIM) using Bray–Curtis distance with 999 permutations in the *vegan* package under R software (Oksanen et al., 2020) was used to test for differences in bacterial community among vegetation sites. The Bray–Curtis distance quantifies the compositional dissimilarity of the bacterial community. The R (version 4.0.5) vegan package was used to create a Bray–Curtis dissimilarity matrix (based on OTU reads) for statistical analyses (Oksanen et al., 2020). To simplify

215 further analyses, OTU data counts for each sample were selected based on the
216 relationship with appropriate sample brGDGT compounds ($R > 0.7$) using a custom R
217 script. The selected OTUs were classified to the phylum level (the Acidobacteria
218 phylum was divided into the class level). The null hypothesis of ANOSIM is "no
219 difference" in community composition between sites and plots. The similarity
220 coefficient $R = 1$ indicates complete separation, and $R = 0$ represents no separation.
221 Strong differences between groups were indicated by $R > 0.51$. P values, also
222 generated by ANOSIM, indicate significance levels. To infer changes in the bacterial
223 community, nonmetric multidimensional scaling (NMDS) analysis was performed
224 using the metaMDS function of the R package *vegan* (Oksanen et al., 2020). The
225 selected OTUs were converted to a Bray–Curtis distance matrix to make the data
226 accessible for statistical analysis. NMDS has proven to be a useful tool to indicate
227 bacterial community changes (De Jonge et al., 2019).

228 Structural equation models (SEMs) are frequently used to resolve complex
229 multivariate relationships among interrelated variables using a form of path analysis.
230 We undertook piecewise SEMs of our brGDGT proxies with environmental and
231 bacterial data to characterize the statistical relationships and to deduce causal
232 relationships between these variables using *a piecewise SEM* library (Lefcheck et al.,
233 2016). The factor was correlated with proxies that were selected from the correlation
234 plot to explore the links in the SEMs using forward selected explanatory variables. We
235 use absolute Akaike information criterion (AIC) indices to evaluate the performance
236 of the SEMs, where the lowest AIC value among the sets indicate the optimal model.
237 We also used chi-square and Fisher's C statistics and associated p values to evaluate
238 model fit. If $p > 0.5$ in the selected SEM, the model fit the complex relationships

among the data well (Lefcheck et al., 2016).

3. Results

3.1 BrGDGT analysis of samples

The fractional abundance of hexamethylated brGDGTs (IIIa, IIIb and IIIc) was low in all samples (Fig. 2). Rainforest soils (TRF) were characterized by high abundances of tetramethylated brGDGTs (accounting for 82% of brGDGTs), whereas brGDGT IIa and IIIa were the predominant brGDGTs in cold regions with shrub meadows (FSM; 45% and 21%, respectively). The different vegetation zones are spread along an altitudinal gradient where MAAT ranges from -2.38 °C at the highest elevation site, FSM to 18.51°C at the lowest elevation site, TRF. In addition, we observe various ranges in soil pH (4.51 at TCF to 6.27 at EBF), soil water content (5.68% at FCF to 25.60% at FSM), conductivity (26.68 µs/cm at FSM to 83.05 µs/cm at SEBF), among other environmental parameters (see Table 1), all of which could influence the distribution of brGDGTs. In the heat map (Fig. 3a) and PCA (Fig. 3b), samples from different vegetation groups tend to cluster together although there is some overlap between samples from adjacent sites, such as the high elevation sites, FSM and FCF, and the mid-elevation sites, SEBF and TCF. TRF appears to be the only site where the samples cluster separately both in the heatmap and PCA. In the RDA plot, MAAT, mean temperature of months above freezing (MAF) and mean annual soil temperature (Tsoil) are positively correlated with brGDGT Ia, but negatively correlated with IIa and IIIa (Fig. 3c). The pH is positively correlated with cyclopentane-containing pentamethylated and hexamethylated brGDGTs, including

IIb, IIc, IIIb and IIIc.

3.2 Genetic data

We selected a strong correlation ($R > 0.7$) between the relative abundance of brGDGTs and OTU-specific DNA concentration (Figs. 4a–4f). There were more than 264 OTUs correlated with IIb, 46 OTUs from Acidobacteria, and 2 and 27 OTUs with Ia and Ib, respectively. The bacterial community composition in our samples was dominated by 12 phyla, of which Proteobacteria (53.30%), Acidobacteria (19.91%), Nitrospirae (2.88%), Bacteroidetes (2.12%), Actinobacteria (2.04%), and Verrucomicrobia (1.59%) are the most abundant phyla. More than half of the OTUs displayed a strong relationship with brGDGTs belonging to Proteobacteria and Acidobacteria (Figs. 4a-f). Among the Acidobacteria, subdivision 6 and subdivision 7 were relatively abundant in our samples (Fig. 4h). The analysis of bacterial community similarities (ANOSIM-$R = 0.381$; $p < 0.001$) confirms that the bacterial community composition differs between vegetation types (Fig. 4i).

3.3 Relationships among environmental variables and brGDGTs at different vegetation sites

Our dataset contains soil samples from fourteen sample sites with six vegetation types that range from -2.38 to 18.92 °C in MAAT, from 5.14 to 18.92 °C in MAF, and from 704 to 3760 m in elevation. Both MAAT and MAF at each site were negatively correlated with elevation ($R = -0.99$ and -0.98, respectively). The pH for our samples ranged from 3.85 to 7.08, with an average value of 5.31, suggesting that most of our samples were acidic (Table 1). The MBT′ values in our samples varied from 0.26 to

0.85 (0.51 on average), and CBT varied from 0.44 to 2.69 (1.07 on average). Generally, the reconstructed MAAT (MAATre) was positively correlated with the observed MAAT (R = 0.73) and MAF (R = 0.77). The brGDGT-derived MAAT overestimates temperature at sites above 2000 m, i.e., SEBF, TCF, FCF, and FSM (Fig. 5c). BrGDGT-derived MAF temperatures, however, do not show this warm bias and fall closer to observed temperature estimates (Fig. 5d). At sites below 2000 m (EBF and TRF), mean annual soil temperatures are colder than MAAT and MAF, whereas at sites above 2000 m (SEBF, TCF, FCF and FSM) soil temperatures are warmer than MAAT and a little colder than MAF (Fig. 5e).

4. Discussion

4.1 Soil bacterial community composition and brGDGT changes

So far the precursors of brGDGTs, ether- and ester-linked iso-diabolic acid (IDA), have only been identified in Acidobacteria cultures (Sinninghe Damsté et al., 2018). Previous studies based on brGDGT distributions, stereochemistry and subsequent culture experiments have so far only identified subdivisions 1, 3, 4 and 6 of the Acidobacteria phylum as brGDGT producers (Sinninghe Damsté et al., 2018; Sinninghe Damsté et al., 2014; Sinninghe Damsté et al., 2011). We compared brGDGT distributions with bacterial community compositions at our study sites to identify potential brGDGT producers (Fig. 4), following the approaches of Weber et al. (2018) and Wu et al. (2021). Similar to previous studies, we observed the strongest correlation between brGDGTs (Ib, Ic, IIb and IIIb) and OTUs belonging to the Acidobacteria phylum in our samples (R is 0.72, 0.57, 0.77 and 0.66 respectively; Fig.

S2). In our samples, GP 6 from the Acidobacteria phylum was the most abundant (49.93% of Acidobacteria), followed by GP 7 (16.00%), 5 (14.60%), 17 (12.71%) and 4 (1.72%). A previous study found that subdivisions 4 and 6 Acidobacteria are potential producers of cyclopentane-containing 5-methyl and 6-methyl brGDGTs, respectively (De Jonge et al., 2021). Cyclopentane-containing brGDGTs (Ib, IIb, IIIb, Ic, IIc, IIIc) were significantly and positively correlated with GP 4 (unicyclic including Ib, IIb, IIIb: $R = 0.76$, $p < 0.01$; bicyclic including Ic, IIc and IIIc: $R = 0.59$, $p < 0.01$) but not GP 6. In our study we failed to separate 5-methyl and 6-methyl brGDGTs, and therefore we cannot correlate GP 6 with 6-methyl brGDGTs, especially if they are present in low abundance.

We found the relative abundance of brGDGT-related GP 4 Acidobacteria was less abundant than GP 6 Acidobacteria in our samples. The soil pH effect on the Acidobacteria community is well documented; for example, subdivisions 4, 6, 7 and 17 increase in soils with an increase in soil pH (Kielak et al., 2016; Sinninghe Damsté et al., 2018). Among the Acidobacteria in our samples, GP 4 increased with increased soil pH, while GP 5 decreased with high pH-levels (Fig. 6). GP 6, however, showed no response to soil temperature or pH. The second dominant strain, GP 7, was negatively correlated with soil temperature and positively correlated with pH. Subdivision 4 is the only subdivision, so far, that was shown to produce 5-methyl iso-diabolic acid (Sinninghe Damsté et al., 2018). The relative abundance of GP 4 was significantly related to soil pH ($R = 0.70$, $p < 0.01$; Fig. 6).

The other five main phyla present in our samples also covary with temperature and pH changes (Fig. 6). Of these phyla, we found that cyclic (Ib, IIb and IIIb) and bicyclic compounds (Ic, IIc and IIIc) are positively correlated with the Proteobacteria

phylum in our samples (R is 0.55, 0.71 and 0.59; 0.46, 0.31 and 0.40 respectively, $p < 0.01$), while noncyclic compounds (Ia, IIa and IIIa) show negative or no relationship with the OTU data (R is -0.23, -0.04 and -0.11, Fig. S2). The subclass of Proteobacteria (α-Proteobacteria and β-Proteobacteria) show the strongest negative relationship with soil temperature ($R = 0.60$ and 0.59, $p < 0.01$, respectively), while γ-Proteobacteria are positively correlated with soil temperature ($R = 0.47$, $p < 0.01$). The relationship between γ-Proteobacteria and soil temperature is opposite to that observed in the inner Mongolia transect (Guo et al., 2022). This dissimilarity may stem from γ-Proteobacteria at high pH and low pH show an opposite response to temperature. In the low pH values ($pH < 7.5$) and high humidity from our study sites, the relative abundance of γ-Proteobacteria increased with increasing temperature. In contrast, in the high pH values ($pH > 7.5$) and more arid conditions from inner Mongolia, the relative abundance of γ-Proteobacteria increased with decreasing temperature (Guo et al., 2022). Certain δ-Proteobacteria were shown to transfer the formation of the ether bond gene (Sinninghe Damsté et al. (2018), which are precursors to brGDGTs. Along with Acidobacteria, our results suggest that members of the Proteobacteria phylum likely contribute to brGDGT production.

Actinobacteria was present at all of our study sites (Fig. 4g), and is correlated with brGDGT Ib, IIb, and IIIb (Figs. 4a – 4f). A previous study identified intact polar lipids (IPLs) of brGDGTs in the membrane of Actinobacteria (Liu et al., 2010), making this a likely candidate for brGDGT production at our study sites. In our samples, the relative abundance of Actinobacteria is positively correlated with soil pH ($R = 0.52$, $p < 0.01$), which contrasts with previous reports from Mongolian soils where the relative abundance of the Actinobacteria phylum was negatively correlated

with pH (Guo et al., 2022). The contrast may result from the different pH ranges at these two sample sites (pH of 7.7 to 9.9 in Mongolia and pH 3.85 to 7.08 in our samples) and a difference in the dominant suborders (samples in Mongolia were dominated by Thermoleophilia, Actinomycetales and Nitriliruptoria; in our samples Acidimicrobiales, Actinomycetales and Solirubrobacterales were dominant). The shift in the bacterial community due to pH changes responds differently to temperature changes. Thus, we propose that soil pH needs to be considered when performing brGDGT-based climate reconstructions.

Both Bacteriodetes and Nitrospira are positively correlated with pH ($R = 0.41$ and 0.54, respectively; $p < 0.01$; Fig. 6). The relative abundance of Nitrospira is also positively correlated with brGDGTs IIb and IIIb ($R = 0.49$ and 0.36, respectively; $p < 0.01$; Fig S2), and negatively correlated with brGDGT Ic ($R = 0.41$; $p < 0.01$). De Jonge et al. (2021) found the highest concentrations of brGDGT Ic in soils with high autotrophic nitrification rates. However, we do not observe any correlations between Nitrospira and TN in Tibetan soils. The relative abundance of Bacteroidetes is positively correlated with brGDGTs Ib and Ic ($R = 0.44$ and 0.37; $p < 0.01$). Although the relationship between brGDGTs and the Bacteroidetes phylum has not yet been reported, members of Bacteroidetes are widely distributed in marine and terrestrial environments (Buckley and Schmidt, 2003; Cottrell and Kirchman, 2000), and thus could be another potential source for the ubiquitous brGDGTs.

Though Verrucomicrobia has not been reported to synthesize brGDGTs, previous work found a strong correlation between Verrucomicrobia and 5-methyl brGDGTs in Mongolian soils (Guo et al., 2022). In our study, the Verrucomicrobia phylum at our sites, is significantly and positively correlated to soil temperature ($R =$

0.65, $p < 0.01$) , and positively related to pH ($R = 0.33$, $p < 0.01$) which differs from previous studies on soils (Guo et al., 2022). The relative abundance of Verrucomicrobia in our samples was positively correlated with Ia ($R = 0.58$, $p < 0.01$) and negatively correlated to IIa and IIc ($R = 0.64$, $p < 0.01$; $R = 0.36$, $p < 0.01$). Verrucomicrobia have the same aerobic heterotrophic lifestyles as known brGDGT producers belonging to the phylum Acidobacteria. Isolates of Verrucomicrobia were shown to produce iso-$C_{15:0}$ fatty acids, which are considered potential precursors for *iso*-diabolic acid and therefore brGDGTs (Sinninghe Damsté et al., 2011). Although we cannot verify that these bacterial phyla are brGDGT-producers, our results indicate Proteobacteria, Verrucomicrobia, Actinobacteria, Nitrospira and Bacteroidetes may be as potential candidates for brGDGT-producers. This information of specific taxonomic groups provides a sight for future laboratory cultivation of bacteria to identify the source of brGDGT producers.

4.2 Effect of biotic and abiotic variables on brGDGT distributions

BrGDGT distributions could be a result of sets of specific bacterial communities that inhabit certain temperature and soil conditions (e.g. pH). Alternatively, brGDGT distributions could be a result of specific bacterial communities that adapt to environmental changes by adjusting the molecular structure of their membrane lipids. De Jonge et al. (2021) demonstrated how a shift in pH resulted in a change in both brGDGT distributions and the bacterial community. Thus, we compared biotic (bacterial community) and abiotic (soil temperatures, TP, pH and conductivity) variables with changes in brGDGT distributions. Our results show that the variation in bacterial communities is strongly related to changes in brGDGT distributions (Fig.

7a). However, the correlation and SEM analyses revealed that noncyclic brGDGTs (Ia, IIa and IIIa) were not directly related to the changes in the bacterial community (Fig. 7b). This effect may stem from the strong positive correlation of Ia with temperatures (i.e., Tsoil, MAF, and MAAT) and the strong negative correlations of IIa and IIIa with temperature (Fig. 7a). Unicyclic and bicyclic brGDGTs (Ib, IIb, IIIb and Ic, IIc, IIIc), in contrast, show a strong negative relationship with bacterial community changes (Fig. 7b &7c). Environmental variables, including temperatures, pH, TP and conductivity, could influence unicyclic and bicyclic brGDGTs (Figs. 7c and 7d). Although cyclic brGDGTs are positively correlated with pH, as observed in previous studies of global soil datasets (Peterse et al., 2012; Weijers et al., 2007), our study confirms the relationship between cyclopentane-containing brGDGTs and pH is controlled by bacterial community changes. In this case, increasing levels in pH levels result in changes in the bacterial community of specific phyla (Proteobacteria, Acidobacteria, Nitrospirae, Bacteroidetes and Actinobacteria) and corresponding increase in the relative abundance of cyclic brGDGTs (Ib, IIb, IIIb, Ic, IIc and IIIc). These findings suggest that calibrations including cyclic brGDGTs should consider the effects of bacterial community shifts on brGDGTs distributions.

4.3 Vegetation effects on brGDGT distributions and bacterial communities: implications for paleoclimate reconstructions

In general, the distribution of brGDGTs at our individual sites follow the established relationships between environmental gradients, where noncyclic tetramethylated brGDGTs (Ia) are abundant at a low elevation with high MAAT (Fig. 2). In contrast, high elevation sites with colder MAATs, such as FCF and FSM, are

429 characterized by a higher relative abundance of noncyclic pentamethylated brGDGTs
430 (IIa, Fig. 3b). Similarly, noncyclic pentamethylated brGDGT IIa were also found in
431 higher abundance in southern Tibetan soils (Bai et al., 2018), inner Mongolia (Guo et
432 al., 2022), and the Chinese Tianshan Mountains (Duan et al., 2020). This suggests that
433 the spatial variation in the relative abundance of brGDGTs is not only linked to
434 temperature or pH, but could result from changes in the bacterial community that are
435 responding to other environmental factors or niche partitioning due to differences in
436 vegetation, for example, pH, oxygen limitation, and cation exchange capacity
437 (Halamka et al., 2021; Halffman et al., 2022). The low relative abundance of IIIa in
438 our samples (Fig. 2a) may respond to redox condition result from water content.
439 Previous environmental observations found that the relative abundance of IIIa is
440 related to changes in oxygen content (Pei et al., 2021; Weber et al., 2018; Yao et al.,
441 2020). Alternatively, brGDGT production likely increases during the summer months,
442 particularly at sites with large seasonal variations (Crampton-Flood et al., 2020). All
443 these factors could contribute to the residual scatter observed in global soil brGDGT
444 calibrations with temperature.

445 At sites above 2500 m in our study sites, there is a warm-bias in brGDGT-based
446 reconstructed temperatures, predicting temperatures up to 5 °C warmer than observed
447 temperatures (Fig. 5c). In contrast, the brGDGT-based temperature reconstructions at
448 the low elevation sites are in line with observed MAAT (Fig. 5c). However, the
449 reconstructed temperature offset with MAF greatly decreased at high altitude sites
450 (Fig. 5d). At the lower elevation sites and warmer regions (TRF and EBF), the mean
451 value of MAAT in these regions was about ~2 °C warmer than Tsoil (Fig. 5e). At
452 these sites, the densely vegetated areas would block radiation inputs to the soil,

453 leading to on average cooler soil temperatures than air temperatures (De Frenne et al.,
454 2021). A similar phenomenon was observed in tropical regions where densely
455 vegetated sites contribute to cooler soil temperatures, and therefore colder brGDGT-
456 based reconstructions relative to the MAAT (Figs. 8a & 8b). At high altitudes (SEBF,
457 TCF and FCF), however, Tsoil was about 1-5 °C higher than MAAT year-round, with
458 the warmest Tsoil values recorded at the shrub meadow site (Tsoil ~5 °C warmer than
459 MAAT). Our results are in agreement with the previous study which compared both
460 Worldclim-derived air temperature and *in-situ* soil temperature with brGDGT-derived
461 temperatures in the northeastern Tibetan Plateau, China and found that soil brGDGTs
462 directly respond to soil temperature variations (Wang and Liu, 2021).
463 To test whether the global brGDGT-derived temperature that was developed
464 using the new method confirms our local observation of vegetation-effects on
465 brGDGT-derived temperatures, we use previously published global soil datasets
466 compiled by Crampton-Flood et al. (2020) and global soil brGDGT calibrations (De
467 Jonge et al., 2014; Naafs et al., 2017a) to reconstruct local temperatures. The results
468 show that the residual value between Tsoil and MAAT match the pattern of bias
469 between reconstructed temperature and MAAT from low latitude to high latitude (Fig.
470 8), and that the residual temperature between soil and air temperature may partly
471 result from vegetation. Vegetation-induced changes in brGDGT distributions have
472 been widely observed in previous studies (Liang et al., 2019; Wang et al., 2020). In
473 addition, we found that there is a significant difference in bacterial communities with
474 vegetation type (ANOSIM, $R = 0.381$, $P < 0.001$), suggesting vegetation-induced
475 changes in brGDGT distribution in soils in response to microbial communities.
476 Changes in plants over time could cause a large shift in soil pH and nutrients (Weijers

et al., 2011; Wu et al., 2020). For instance, in wet meadows degradation rates are high, leading to a decrease in aboveground biomass and soil nutrient content (Wu et al., 2020). Peaple et al. (2022) found in situ measurements of soil temperatures are warmer than interpolated mean annual temperatures in most grassland plains in eastern Africa. Similarly, the vegetation change from Carex to Sphagnum in Swiss peat contributed to the variations in brGDGTs, consistent with a decrease in pH from 8 to 4 (Weijers et al., 2011). Thus, the implication for a paleoclimate proxy is that reconstructed soil temperature using brGDGTs should be interpreted with caution, as changes in vegetation could lead to a bacterial community shift and therefore a change in the cyclopentane brGDGT distribution.

Soil pH impacts the bacterial community, which in turn influences brGDGT distributions at experimental sites (De Jonge et al., 2021). We further found that pH and nutrients significantly impacted both the bacterial community and cyclized brGDGTs. Due to the significant correlation of pH and nutrients with the bacterial community in our soil samples (Fig. 7c), changes in pH and nutrient records may be related to bacterial community changes in paleoclimate reconstructions and changes in pH has a stronger influence. Although molecular dynamics simulations of pure monolayer membranes demonstrate that the brGDGT paleothermometer is based on a homeoviscous adaption, it should be noted that in reality the bacterial membrane consists brGDGT lipid bilayer (Naafs et al., 2021). The effect of shift in the bacterial community on brGDGT distribution should not be ignored. Therefore, to develop a robust reconstructed temperature based on brGDGTs, future efforts on brGDGTs should focus on the relationship between the bacterial communities and other environmental variables.

Conclusion

We test the suitability of brGDGTs as a temperature proxy in soils along a vegetation and altitudinal gradient on the southeastern Tibetan Plateau. A comparison of the bacterial community composition with brGDGTs revealed that Acidobacteria may not be the only producers of brGDGTs in our samples. Instead, Proteobacteria, Nitrospira, Bacteroidetes, Actinobacteria, and Verrucomicrobia could be potential candidates as brGDGT producers. Using the Peterse et al. (2012) soil calibration, we find that reconstructed temperatures are correlated with observed MAAT below 2500 m; however, at sites above 2500 m we observe a warm bias. The temperature offsets at our study sites could either be explained by differences in seasonality or vegetation, which could influence the soil chemistry and the amount of radiation reaching the soil. However, at the same study sites, we observe distinct changes in the bacterial communities and shifts in brGDGT distributions across the vegetation zones. Changes in temperature, pH, conductivity and TP directly influence the bacterial community and, therefore, the distribution of cyclopentane-containing brGDGTs. We found that noncyclic brGDGTs may have a strong positive relationship with temperature but are likely not related to specific changes in the lipid membrane independent of the bacteria that produce these brGDGTs in our samples. Finally, we found that the residual value from previously published brGDGT datasets between Tsoil and MAAT match the pattern of bias between brGDGT-derived temperature and MAAT from low latitude to high latitude, suggesting that brGDGT temperature reconstructions directly respond to soil temperatures rather than air temperatures.

Acknowledgments

The authors would like to thank the editors and two anonymous reviewers for their contractive comments. We also thank to Drs. Keshao Liu and Ang Hu for advice. This study was supported by the National Natural Science Foundation of China (Grant NO. 42101158, 41871066, 41471055); the Second Tibetan Plateau Scientific Expedition and Research Program (Grant No. 2019QZKK0503). We also thank the Southeast Tibet Observation and Research Station for the Alpine Environment,CAS, and Motuo Observation and Research Center for Earth Landscape and Earth System, CAS, for field sampling.

Figure Captions

Figure 1. Sampling sites: (a) Location of the 14 sampling sites at different altitudes. (b) Characterization of plant communities at different altitudes.

Figure 2. Bar plot of the relative abundance of brGDGTs in soils (a). The fractional abundance of summed tetramethylated, pentamethylated, and hexamethylated brGDGTs in our soils (b).

Figure 3. Heatmap with the clustering method (Euclidean distance) of the relative abundance of brGDGTs in soils with different vegetation types (a). Principal component analysis (PCA) of the standardized fractional abundance of brGDGTs (b) and redundancy analysis (RDA) for environmental variables and the relative abundance of brGDGTs (c).

548

549 Figure 4. Diversity of OTUs that have a strong correlation with one of the major
550 brGDGTs in our samples. Correlation analysis was performed between the
551 concentration of each OTU and the relative abundance of individual brGDGT
552 compounds. Highly correlated OTUs are displayed at the phylum level (large pie
553 charts; a–f) and as subdivisions of Acidobacteria (small pie charts; a-f). “n” refers to
554 the number of OTUs in each chart. Each pie piece was estimated based on OTU-
555 specific DNA concentration of phylum (or subdivisions of Acidobacteria) account for
556 total OTU-specific DNA concentration. The relative abundance of OTU-specific DNA
557 concentration at the phylum level (g) and at the subdivisions of Acidobacteria level
558 (h). ANOSIM with R values and their associated significance (P) between sites and
559 between plot differences in six different vegetation sites in this study based on the
560 selected most correlated OTU concentrations (i). p levels <1.0 indicate significant
561 differences in species composition.

562

563 Figure 5. Violin plots of MAAT and reconstructed temperature among six
564 different vegetation sites, including (a) MAAT, (b) reconstructed mean annual air
565 temperatures based on brGDGTs (MAATre) based on brGDGTs [Eq. 3], (c) the offset
566 between MAATre and MAAT and (d) the offset between MAATre and MAF. Dashed
567 line is the 0 °C for the bias of temperatures. (e) The standard deviations of MAF (dark
568 grey), MAAT (light grey) and Tsoil (red) in our study sites. The plots are ordered
569 according to the altitude and vegetation from the lowest altitude (TRF, ~900 m) to the
570 highest altitude (FSM, ~3700 m).

571

572 Figure 6. Scatter plot of the relative abundance of bacterial phyla with mean
573 annual soil temperature and pH. The linear regression lines of correlations with $p <$
574 0.05, the 95% confidence intervals are displayed by the gray shaded area. Values
575 below the limit of quantification are not included in linear regression.
576
577 Figure 7. Stepwise forward selection regression explained the variation between
578 brGDGT fractional abundance and environmental variables (a; top). Spearman
579 correlation matrix for brGDGT fractional abundance with environmental variables (a;
580 bottom). The significant value *** significant at the 0.1% level, and ** significant at
581 the 1% level. Key driver of brGDGT fractional abundance. Structural equation models
582 showing the potential drivers of noncyclic brGDGTs (Ia, IIa and IIIa; b), unicyclic
583 brGDGTs (Ib, IIb and IIIb; c) and bicyclic brGDGTs (Ic, IIc and IIIc; d). Arrow color
584 corresponds to positive (red) or negative (blue) of the path coefficient. BC initial for
585 bacterial community change from NMDS1 scores, Tsoil initial for mean annual soil
586 temperature and Cond initial for conductivity.
587
588 Figure 8. The offset of reconstructed temperatures, MAF and mean annual soil
589 temperatures with MAAT from previous published global datasets compiled by
590 Crampton-Flood et al. (2020). (a) the offset of brGDGT-reconstructed temperatures
591 based on a calibration developed by (Naafs et al., 2017a) and MAAT; (b) the offset of
592 brGDGT-reconstructed temperatures based on calibration from (De Jonge et al., 2014)
593 and MAAT; (c) the offset of MAF and MAAT; (d) the offset of mean annual soil
594 temperatures and MAAT. The black dots mean no temperature data.
595

Table

Table 1. Descriptive statistics of environmental variables in our study sites, including tropical rainforest zone (TRF), evergreen broad-leaved forest zone (EBF), semi-evergreen broad-leaved forest zone (SEBF); temperate mixed coniferous broad-leaved forest zone (TCF), frigid-temperate coniferous forest zones (FCF); and frigid shrubs and meadow zone (FSM).

	TRF	EBF	SEBF	TCF	FCF	FSM
Elevation	892.33±163.14	1626.25±183.96	2299±113.02	2781.67±138.19	3359±186.71	3760
Dominant vegetation type	*Altingiaexcelsa* and *Terminalia myriocarpa*	*Castanopsishystrix*, *Altingiaexcelsa*, *Castanopsisechidnocarpa*, *Cyclobalanopsisgambleana*, *Lithocarpusxizangensis*, *Quercuslodicosa* and *Cyclobalanopsisoxyodonare*	*Quercuslanata* and *Cyclobalanopsislamellosa*	*Tsugadumosa*	*Larixspeciosa* and *Abiesdelavayi*	*scattered shrubs*
MAAT (°C)	18.51±0.38	12.31±0.4	9.24±1.04	5.56±0.33	1.61±1.78	-2.38
MAF T (°C)	18.51±0.38	12.31±0.4	10.15±0.08	9.03±0.12	6.95±0.96	5.14
Tsoil (°C)	17.38±0.55	9.93±0.05	8.89±0.1	7.9±1.1	5.46±1.13	2.9
Water content (%)	68.31±6.52	83.54±28.06	76.98±51.24	96.72±73.75	64.95±63.08	28.8
pH	5.07±0	6.28±0.57	5.63±0.45	4.98±1.13	4.79±0.59	5
Conductivity (μS/cm)	60.28±20.32	62.47±9.9	35.76±10.59	57.5±32.9	40.09±30.07	22.7
TOC (%)	0.02±0	0.02±0	0.02±0	0.02±0	0.02±0	0.02
TN	6.1±1.69	5.3±3.19	3.82±2.62	4.51±1.67	4.53±3.17	1.91±2.19
TP	1.99±0.26	3.24±0.76	2.29±0.64	1.38±0.45	2.41±0.71	1.9±0.66

603

References

Bai, Y., Chen, C., Xu, Q., Fang, X., 2018. Paleoaltimetry Potentiality of Branched GDGTs From Southern Tibet. Geochemistry, Geophysics, Geosystems 19, 551-564.

Baxter, A.J., Hopmans, E.C., Russell, J.M., Sinninghe Damsté, J.S., 2019. Bacterial GMGTs in East African lake sediments: Their potential as palaeotemperature indicators. Geochimica et Cosmochimica Acta 259, 155-169.

Bremner, J., 1960. Determination of nitrogen in soil by the Kjeldahl method. The Journal of Agricultural Science 55, 11-33.

Buckley, D.H., Schmidt, T.M., 2003. Diversity and dynamics of microbial communities in soils from agro-ecosystems. Environmental Microbiology 5, 441-452.

Caporaso, J.G., Kuczynski, J., Stombaugh, J., Bittinger, K., Bushman, F.D., Costello, E.K., Fierer, N., Peña, A.G., Goodrich, J.K., Gordon, J.I., 2010. QIIME allows analysis of high-throughput community sequencing data. Nature methods 7, 335-336.

Chen, C., Bai, Y., Fang, X., Zhuang, G., Khodzhiev, A., Bai, X., Murodov, A., 2021. Evaluating the potential of soil bacterial tetraether proxies in westerlies dominating western Pamirs, Tajikistan and implications for paleoenvironmental reconstructions. Chemical Geology 559, 119908.

Cole, J.R., Wang, Q., Cardenas, E., Fish, J., Chai, B., Farris, R.J., Kulam-Syed-Mohideen, A., McGarrell, D.M., Marsh, T., Garrity, G.M., 2009. The Ribosomal Database Project: improved alignments and new tools for rRNA analysis. Nucleic acids research 37, D141-D145.

Cottrell, M.T., Kirchman, D.L., 2000. Community composition of marine bacterioplankton determined by 16S rRNA gene clone libraries and fluorescence in situ hybridization. Applied and Environmental Microbiology 66, 5116-5122.

Crampton-Flood, E.D., Tierney, J.E., Peterse, F., Kirkels, F.M., Sinninghe Damsté, J.S., 2020. BayMBT: A Bayesian calibration model for branched glycerol dialkyl glycerol tetraethers in soils and peats. Geochimica et Cosmochimica Acta 268, 142-159.

Crampton-Flood, E.D., van der Weijst, C.M., van der Molen, G., Bouquet, M., Yedema, Y., Donders, T.H., Sangiorgi, F., Sluijs, A., Sinninghe Damsté, J.S., Peterse, F., 2021. Identifying marine and freshwater overprints on soil-derived branched GDGT temperature signals in Pliocene Mississippi and Amazon River

639 fan sediments. Organic Geochemistry 154, 104200.
640 Dang, X., Ding, W., Yang, H., Pancost, R.D., Naafs, B.D.A., Xue, J., Lin, X., Lu, J.,
641 Xie, S., 2018. Different temperature dependence of the bacterial brGDGT
642 isomers in 35 Chinese lake sediments compared to that in soils. Organic
643 Geochemistry 119, 72-79.
644 De Frenne, P., Lenoir, J., Luoto, M., Scheffers, B.R., Zellweger, F., Aalto, J., Ashcroft,
645 M.B., Christiansen, D.M., Decocq, G., De Pauw, K., Govaert, S., Greiser, C.,
646 Gril, E., Hampe, A., Jucker, T., Klinges, D.H., Koelemeijer, I.A., Lembrechts,
647 J.J., Marrec, R., Meeussen, C., Ogée, J., Tyystjärvi, V., Vangansbeke, P.,
648 Hylander, K., 2021. Forest microclimates and climate change: Importance,
649 drivers and future research agenda. Global Change Biology 27, 2279-2297.
650 De Jonge, C., Hopmans, E.C., Zell, C.I., Kim, J.-H., Schouten, S., Damsté, J.S.S.,
651 2014. Occurrence and abundance of 6-methyl branched glycerol dialkyl glycerol
652 tetraethers in soils: Implications for palaeoclimate reconstruction. Geochimica et
653 Cosmochimica Acta 141, 97-112.
654 De Jonge, C., Kuramae, E.E., Radujković, D., Weedon, J.T., Janssens, I.A., Peterse,
655 F., 2021. The influence of soil chemistry on branched tetraether lipids in mid-
656 and high latitude soils: Implications for brGDGT- based paleothermometry.
657 Geochimica et Cosmochimica Acta 310, 95-112.
658 De Jonge, C., Radujković, D., Sigurdsson, B.D., Weedon, J.T., Janssens, I., Peterse, F.,
659 2019. Lipid biomarker temperature proxy responds to abrupt shift in the bacterial
660 community composition in geothermally heated soils. Organic Geochemistry
661 137, 103897.
662 Dick, W., Tabatabai, M., 1977. An alkaline oxidation method for determination of
663 total phosphorus in soils. Soil Science Society of America Journal 41, 511-514.
664 Duan, Y., Sun, Q., Werne, J.P., Yang, H., Jia, J., Wang, L., Xie, H., Chen, F., 2020.
665 Soil pH Dominates the Distributions of Both 5- and 6-Methyl Branched
666 Tetraethers in Arid Regions. Journal of Geophysical Research: Biogeosciences
667 125, e2019JG005356.
668 Edgar, R.C., 2013. UPARSE: highly accurate OTU sequences from microbial
669 amplicon reads. Nature methods 10, 996-998.
670 Edgar, R.C., Haas, B.J., Clemente, J.C., Quince, C., Knight, R., 2011. UCHIME
671 improves sensitivity and speed of chimera detection. Bioinformatics 27, 2194-
672 2200.
673 Fick, S.E., Hijmans, R.J., 2017. WorldClim 2: new 1-km spatial resolution climate
674 surfaces for global land areas. International Journal of Climatology 37, 4302-

675 4315.
676 Gu, Z., Eils, R., Schlesner, M., 2016. Complex heatmaps reveal patterns and
677 correlations in multidimensional genomic data. Bioinformatics 32, 2847-2849.
678 Guo, J., Ma, T., Liu, N., Zhang, X., Hu, H., Ma, W., Wang, Z., Feng, X., Peterse, F.,
679 2022. Soil pH and aridity influence distributions of branched tetraether lipids in
680 grassland soils along an aridity transect. Organic Geochemistry, 104347.
681 Halamka, T.A., McFarlin, J.M., Younkin, A.D., Depoy, J., Dildar, N., Kopf, S.H.,
682 2021. Oxygen limitation can trigger the production of branched GDGTs in
683 culture. Geochemical Perspectives Letters 19, 36-39.
684 Halffman, R., Lembrechts, J., Radujković, D., De Gruyter, J., Nijs, I., De Jonge, C.,
685 2022. Soil chemistry, temperature and bacterial community composition drive
686 brGDGT distributions along a subarctic elevation gradient. Organic
687 Geochemistry 163, 104346.
688 Hopmans, E.C., Schouten, S., Sinninghe Damsté, J.S., 2016. The effect of improved
689 chromatography on GDGT-based palaeoproxies. Organic Geochemistry 93, 1-6.
690 Hu, A., Wang, J., Sun, H., Niu, B., Si, G., Wang, J., Yeh, C.-F., Zhu, X., Lu, X., Zhou,
691 J., Yang, Y., Ren, M., Hu, Y., Dong, H., Zhang, G., 2020. Mountain biodiversity
692 and ecosystem functions: interplay between geology and contemporary
693 environments. The ISME Journal 14, 931-944.
694 Husson, F., Josse, J., Le, S., Mazet, J., Husson, M.F., 2016. Package 'FactoMineR'.
695 An R package 96, 698.
696 Inglis, G.N., Collinson, M.E., Riegel, W., Wilde, V., Farnsworth, A., Lunt, D.J.,
697 Valdes, P., Robson, B.E., Scott, A.C., Lenz, O.K., 2017. Mid-latitude continental
698 temperatures through the early Eocene in western Europe. Earth and Planetary
699 Science Letters 460, 86-96.
700 Kielak, A.M., Scheublin, T.R., Mendes, L.W., Van Veen, J.A., Kuramae, E.E., 2016.
701 Bacterial community succession in pine-wood decomposition. Frontiers in
702 microbiology 7, 231.
703 Lefcheck, J., Byrnes, J., Grace, J., 2016. Package 'piecewiseSEM'. R package version
704 1.
705 Lembrechts, J.J., van den Hoogen, J., Aalto, J., Ashcroft, M.B., De Frenne, P.,
706 Kemppinen, J., Kopecký, M., Luoto, M., Maclean, I.M.D., Crowther, T.W.,
707 Bailey, J.J., Haesen, S., Klinges, D.H., Niittynen, P., Scheffers, B.R., Van
708 Meerbeek, K., Aartsma, P., Abdalaze, O., Abedi, M., Aerts, R., Ahmadian, N.,
709 Ahrends, A., Alatalo, J.M., Alexander, J.M., Allonsius, C.N., Altman, J.,
710 Ammann, C., Andres, C., Andrews, C., Ardö, J., Arriga, N., Arzac, A., Aschero,

V., Assis, R.L., Assmann, J.J., Bader, M.Y., Bahalkeh, K., Barančok, P., Barrio, I.C., Barros, A., Barthel, M., Basham, E.W., Bauters, M., Bazzichetto, M., Marchesini, L.B., Bell, M.C., Benavides, J.C., Benito Alonso, J.L., Berauer, B.J., Bjerke, J.W., Björk, R.G., Björkman, M.P., Björnsdóttir, K., Blonder, B., Boeckx, P., Boike, J., Bokhorst, S., Brum, B.N.S., Brůna, J., Buchmann, N., Buysse, P., Camargo, J.L., Campoe, O.C., Candan, O., Canessa, R., Cannone, N., Carbognani, M., Carnicer, J., Casanova-Katny, A., Cesarz, S., Chojnicki, B., Choler, P., Chown, S.L., Cifuentes, E.F., Čiliak, M., Contador, T., Convey, P., Cooper, E.J., Cremonese, E., Curasi, S.R., Curtis, R., Cutini, M., Dahlberg, C.J., Daskalova, G.N., de Pablo, M.A., Della Chiesa, S., Dengler, J., Deronde, B., Descombes, P., Di Cecco, V., Di Musciano, M., Dick, J., Dimarco, R.D., Dolezal, J., Dorrepaal, E., Dušek, J., Eisenhauer, N., Eklundh, L., Erickson, T.E., Erschbamer, B., Eugster, W., Ewers, R.M., Exton, D.A., Fanin, N., Fazlioglu, F., Feigenwinter, I., Fenu, G., Ferlian, O., Fernández Calzado, M.R., Fernández-Pascual, E., Finckh, M., Higgens, R.F., Forte, T.a.G.W., Freeman, E.C., Frei, E.R., Fuentes-Lillo, E., García, R.A., García, M.B., Géron, C., Gharun, M., Ghosn, D., Gigauri, K., Gobin, A., Goded, I., Goeckede, M., Gottschall, F., Goulding, K., Govaert, S., Graae, B.J., Greenwood, S., Greiser, C., Grelle, A., Guénard, B., Guglielmin, M., Guillemot, J., Haase, P., Haider, S., Halbritter, A.H., Hamid, M., Hammerle, A., Hampe, A., Haugum, S.V., Hederová, L., Heinesch, B., Helfter, C., Hepenstrick, D., Herberich, M., Herbst, M., Hermanutz, L., Hik, D.S., Hoffrén, R., Homeier, J., Hörtnagl, L., Høye, T.T., Hrbacek, F., Hylander, K., Iwata, H., Jackowicz-Korczynski, M.A., Jactel, H., Järveoja, J., Jastrzębowski, S., Jentsch, A., Jiménez, J.J., Jónsdóttir, I.S., Jucker, T., Jump, A.S., Juszczak, R., Kanka, R., Kašpar, V., Kazakis, G., Kelly, J., Khuroo, A.A., Klemedtsson, L., Klisz, M., Kljun, N., Knohl, A., Kobler, J., Kollár, J., Kotowska, M.M., Kovács, B., Kreyling, J., Lamprecht, A., Lang, S.I., Larson, C., Larson, K., Laska, K., le Maire, G., Leihy, R.I., Lens, L., Liljebladh, B., Lohila, A., Lorite, J., Loubet, B., Lynn, J., Macek, M., Mackenzie, R., Magliulo, E., Maier, R., Malfasi, F., Máliš, F., Man, M., Manca, G., Manco, A., Manise, T., Manolaki, P., Marciniak, F., Matula, R., Mazzolari, A.C., Medinets, S., Medinets, V., Meeussen, C., Merinero, S., Mesquita, R.d.C.G., Meusburger, K., Meysman, F.J.R., Michaletz, S.T., Milbau, A., Moiseev, D., Moiseev, P., Mondoni, A., Monfries, R., Montagnani, L., Moriana-Armendariz, M., Morra di Cella, U., Mörsdorf, M., Mosedale, J.R., Muffler, L., Muñoz-Rojas, M., Myers, J.A., Myers-Smith, I.H., Nagy, L., Nardino, M., Naujokaitis-Lewis, I., Newling,

E., Nicklas, L., Niedrist, G., Niessner, A., Nilsson, M.B., Normand, S., Nosetto, M.D., Nouvellon, Y., Nuñez, M.A., Ogaya, R., Ogée, J., Okello, J., Olejnik, J., Olesen, J.E., Opedal, Ø.H., Orsenigo, S., Palaj, A., Pampuch, T., Panov, A.V., Pärtel, M., Pastor, A., Pauchard, A., Pauli, H., Pavelka, M., Pearse, W.D., Peichl, M., Pellissier, L., Penczykowski, R.M., Penuelas, J., Petit Bon, M., Petraglia, A., Phartyal, S.S., Phoenix, G.K., Pio, C., Pitacco, A., Pitteloud, C., Plichta, R., Porro, F., Portillo-Estrada, M., Poulenard, J., Poyatos, R., Prokushkin, A.S., Puchalka, R., Puşcaş, M., Radujković, D., Randall, K., Ratier Backes, A., Remmele, S., Remmers, W., Renault, D., Risch, A.C., Rixen, C., Robinson, S.A., Robroek, B.J.M., Rocha, A.V., Rossi, C., Rossi, G., Roupsard, O., Rubtsov, A.V., Saccone, P., Sagot, C., Sallo Bravo, J., Santos, C.C., Sarneel, J.M., Scharnweber, T., Schmeddes, J., Schmidt, M., Scholten, T., Schuchardt, M., Schwartz, N., Scott, T., Seeber, J., Segalin de Andrade, A.C., Seipel, T., Semenchuk, P., Senior, R.A., Serra-Diaz, J.M., Sewerniak, P., Shekhar, A., Sidenko, N.V., Siebicke, L., Siegwart Collier, L., Simpson, E., Siqueira, D.P., Sitková, Z., Six, J., Smiljanic, M., Smith, S.W., Smith-Tripp, S., Somers, B., Sørensen, M.V., Souza, J.J.L.L., Souza, B.I., Souza Dias, A., Spasojevic, M.J., Speed, J.D.M., Spicher, F., Stanisci, A., Steinbauer, K., Steinbrecher, R., Steinwandter, M., Stemkovski, M., Stephan, J.G., Stiegler, C., Stoll, S., Svátek, M., Svoboda, M., Tagesson, T., Tanentzap, A.J., Tanneberger, F., Theurillat, J.-P., Thomas, H.J.D., Thomas, A.D., Tielbörger, K., Tomaselli, M., Treier, U.A., Trouillier, M., Turtureanu, P.D., Tutton, R., Tyystjärvi, V.A., Ueyama, M., Ujházy, K., Ujházyová, M., Uogintas, D., Urban, A.V., Urban, J., Urbaniak, M., Ursu, T.-M., Vaccari, F.P., Van de Vondel, S., van den Brink, L., Van Geel, M., Vandvik, V., Vangansbeke, P., Varlagin, A., Veen, G.F., Veenendaal, E., Venn, S.E., Verbeeck, H., Verbrugggen, E., Verheijen, F.G.A., Villar, L., Vitale, L., Vittoz, P., Vives-Ingla, M., von Oppen, J., Walz, J., Wang, R., Wang, Y., Way, R.G., Wedegärtner, R.E.M., Weigel, R., Wild, J., Wilkinson, M., Wilmking, M., Wingate, L., Winkler, M., Wipf, S., Wohlfahrt, G., Xenakis, G., Yang, Y., Yu, Z., Yu, K., Zellweger, F., Zhang, J., Zhang, Z., Zhao, P., Ziemblińska, K., Zimmermann, R., Zong, S., Zyryanov, V.I., Nijs, I., Lenoir, J., 2022. Global maps of soil temperature. Global Change Biology 28, 3110-3144.

Liang, J., Russell, J.M., Xie, H., Lupien, R.L., Si, G., Wang, J., Hou, J., Zhang, G., 2019. Vegetation effects on temperature calibrations of branched glycerol dialkyl glycerol tetraether (brGDGTs) in soils. Organic Geochemistry 127, 1-11.

Liao, S., Wang, K.J., Huang, Y., 2021. Extended chain length alkenoates differentiate

783 three Isochrysidales groups. Organic Geochemistry 161, 104303.
784 Liu, X.-L., Leider, A., Gillespie, A., Gröger, J., Versteegh, G.J., Hinrichs, K.-U., 2010.
785 Identification of polar lipid precursors of the ubiquitous branched GDGT orphan
786 lipids in a peat bog in Northern Germany. Organic Geochemistry 41, 653-660.
787 Naafs, B.D.A., Gallego-Sala, A.V., Inglis, G.N., Pancost, R.D., 2017a. Refining the
788 global branched glycerol dialkyl glycerol tetraether (brGDGT) soil temperature
789 calibration. Organic Geochemistry 106, 48-56.
790 Naafs, B.D.A., Inglis, G.N., Zheng, Y., Amesbury, M., Biester, H., Bindler, R.,
791 Blewett, J., Burrows, M., Del Castillo Torres, D., Chambers, F.M., 2017b.
792 Introducing global peat-specific temperature and pH calibrations based on
793 brGDGT bacterial lipids. Geochimica et Cosmochimica Acta 208, 285-301.
794 Naafs, B.D.A., McCormick, D., Inglis, G., Pancost, R., 2018. Archaeal and bacterial
795 H-GDGTs are abundant in peat and their relative abundance is positively
796 correlated with temperature. Geochimica et Cosmochimica Acta 227, 156-170.
797 Naafs, B.D.A., Oliveira, A.S.F., Mulholland, A.J., 2021. Molecular dynamics
798 simulations support the hypothesis that the brGDGT paleothermometer is based
799 on homeoviscous adaptation. Geochimica et Cosmochimica Acta 312, 44-56.
800 Oksanen, J., Blanchet, F.G., Friendly, M., Kindt, R., Legendre, P., McGlinn, D.,
801 Minchin, P.R., O'Hara, R.B., Gavin L.Simpson, Solymos, P., Stevens, M.H.H.,
802 Szoecs, E., Wagner, H., 2020. vegan: Community Ecology Package. URL:
803 https://CRAN.R-project.org/package=vegan
804 Peaple, M.D., Beverly, E.J., Garza, B., Baker, S., Levin, N.E., Tierney, J.E., Häggi, C.,
805 Feakins, S.J., 2022. Identifying the drivers of GDGT distributions in alkaline soil
806 profiles within the Serengeti ecosystem. Organic Geochemistry, 104433.
807 Pei, H., Zhao, S., Yang, H., Xie, S., 2021. Variation of branched tetraethers with soil
808 depth in relation to non-temperature factors: Implications for paleoclimate
809 reconstruction. Chemical Geology 572, 120211.
810 Peterse, F., van der Meer, J., Schouten, S., Weijers, J.W., Fierer, N., Jackson, R.B.,
811 Kim, J.-H., Damsté, J.S.S., 2012. Revised calibration of the MBT–CBT
812 paleotemperature proxy based on branched tetraether membrane lipids in surface
813 soils. Geochimica et Cosmochimica Acta 96, 215-229.
814 R Core Team, 2021. R: A language and environment for statistical computing. R
815 Foundation for Statistical Computing, Vienna, Austria.
816 Raberg, J.H., Miller Gifford, H., Geirsdóttir, Á., Sepúlveda, J., 2022. Near-universal
817 trends in brGDGT lipid distributions in nature. Science Advances 8, eabm7625.
818 Russell, J.M., Hopmans, E.C., Loomis, S.E., Liang, J., SinninghеDamsté, J.S., 2018.

Distributions of 5-and 6-methyl branched glycerol dialkyl glycerol tetraethers (brGDGTs) in East African lake sediment: Effects of temperature, pH, and new lacustrine paleotemperature calibrations. Organic Geochemistry 117, 56-69.

Sinninghe Damsté, J.S., Rijpstra, W.I.C., Foesel, B.U., Huber, K.J., Overmann, J., Nakagawa, S., Kim, J.J., Dunfield, P.F., Dedysh, S.N., Villanueva, L., 2018. An overview of the occurrence of ether-and ester-linked iso-diabolic acid membrane lipids in microbial cultures of the Acidobacteria: Implications for brGDGT paleoproxies for temperature and pH. Organic Geochemistry 124, 63-76.

Sinninghe Damsté, J.S., Rijpstra, W.I.C., Hopmans, E.C., Foesel, B.U., Wüst, P.K., Overmann, J., Tank, M., Bryant, D.A., Dunfield, P.F., Houghton, K., 2014. Ether- and ester-bound iso-diabolic acid and other lipids in members of Acidobacteria subdivision 4. Applied and Environmental Microbiology 80, 5207-5218.

Sinninghe Damsté, J.S., Rijpstra, W.I.C., Hopmans, E.C., Weijers, J.W., Foesel, B.U., Overmann, J., Dedysh, S.N., 2011. 13, 16-Dimethyl octacosanedioic acid (iso-diabolic acid), a common membrane-spanning lipid of Acidobacteria subdivisions 1 and 3. Applied and environmental microbiology 77, 4147-4154.

Tang, X., Naafs, B.D.A., Pancost, R.D., Liu, Z., Fan, T., Zheng, Y., 2021. Exploring the influences of temperature on “H-Shaped” Glycerol Dialkyl Glycerol Tetraethers in a stratigraphic context: evidence from two peat cores across the late Quaternary. Frontiers in Earth Science 8, 477.

Thompson, A.J., Zhu, J., Poulsen, C.J., Tierney, J.E., Skinner, C.B., 2022. Northern Hemisphere vegetation change drives a Holocene thermal maximum. Science advances 8, eabj6535.

Wang, H., An, Z., Lu, H., Zhao, Z., Liu, W., 2020. Calibrating bacterial tetraether distributions towards in situ soil temperature and application to a loess-paleosol sequence. Quaternary Science Reviews 231, 106172.

Wang, H., Liu, W., 2021. Soil temperature and brGDGTs along an elevation gradient on the northeastern Tibetan Plateau: A test of soil brGDGTs as a proxy for paleoelevation. Chemical Geology 566, 120079.

Wang, M., Hou, J., Duan, Y., Chen, J., Li, X., He, Y., Lee, S.-Y., Chen, F., 2021. Internal feedbacks forced Middle Holocene cooling on the Qinghai-Tibetan Plateau. Boreas 50, 1116-1130.

Weber, Y., Damsté, J.S.S., Zopfi, J., De Jonge, C., Gilli, A., Schubert, C.J., Lepori, F., Lehmann, M.F., Niemann, H., 2018. Redox-dependent niche differentiation provides evidence for multiple bacterial sources of glycerol tetraether lipids in lakes. Proceedings of the National Academy of Sciences 115, 10926-10931.

Weber, Y., De Jonge, C., Rijpstra, W.I.C., Hopmans, E.C., Stadnitskaia, A., Schubert, C.J., Lehmann, M.F., Damsté, J.S.S., Niemann, H., 2015. Identification and carbon isotope composition of a novel branched GDGT isomer in lake sediments: Evidence for lacustrine branched GDGT production. Geochimica et Cosmochimica Acta 154, 118-129.

Weijers, J.W., Schouten, S., van den Donker, J.C., Hopmans, E.C., Sinninghe Damsté, J.S., 2007. Environmental controls on bacterial tetraether membrane lipid distribution in soils. Geochimica et Cosmochimica Acta 71, 703-713.

Weijers, J.W., Steinmann, P., Hopmans, E.C., Schouten, S., Sinninghe Damsté, J.S., 2011. Bacterial tetraether membrane lipids in peat and coal: Testing the MBT–CBT temperature proxy for climate reconstruction. Organic Geochemistry 42, 477-486.

Wu, J., Wang, H., Li, G., Ma, W., Wu, J., Gong, Y., Xu, G., 2020. Vegetation degradation impacts soil nutrients and enzyme activities in wet meadow on the Qinghai-Tibet Plateau. Scientific Reports 10, 21271.

Wu, J., Yang, H., Pancost, R.D., Naafs, B.D.A., Qian, S., Dang, X., Sun, H., Pei, H., Wang, R., Zhao, S., 2021. Variations in dissolved O_2 in a Chinese lake drive changes in microbial communities and impact sedimentary GDGT distributions. Chemical Geology, 120348.

Yang, H., Pancost, R.D., Dang, X., Zhou, X., Evershed, R.P., Xiao, G., Tang, C., Gao, L., Guo, Z., Xie, S., 2014a. Correlations between microbial tetraether lipids and environmental variables in Chinese soils: Optimizing the paleo-reconstructions in semi-arid and arid regions. Geochimica et Cosmochimica Acta 126, 49-69.

Yang, H., Pancost, R.D., Tang, C., Ding, W., Dang, X., Xie, S., 2014b. Distributions of isoprenoid and branched glycerol dialkanol diethers in Chinese surface soils and a loess–paleosol sequence: Implications for the degradation of tetraether lipids. Organic Geochemistry 66, 70-79.

Yao, Y., Zhao, J., Vachula, R.S., Werne, J.P., Wu, J., Song, X., Huang, Y., 2020. Correlation between the ratio of 5-methyl hexamethylated to pentamethylated branched GDGTs (HP5) and water depth reflects redox variations in stratified lakes. Organic Geochemistry 147, 104076.

Zhao, B., Castañeda, I.S., Bradley, R.S., Salacup, J.M., de Wet, G.A., Daniels, W.C., Schneider, T., 2021. Development of an in situ branched GDGT calibration in Lake 578, southern Greenland. Organic Geochemistry 152, 104168.

Highlights

1. Bacterial community and brGDGTs are compared along altitudinal vegetational soils
2. Bacterial community would directly influence cyclopentane-containing brGDGTs
3. Noncyclic brGDGTs have a strong positive relationship with temperature
4. Vegetation influence on brGDGTs reconstruction though changing bacterial community and in situ temperature
5. Soil brGDGT-derived temperatures directly respond to soil temperatures rather than air temperatures

Figure 1

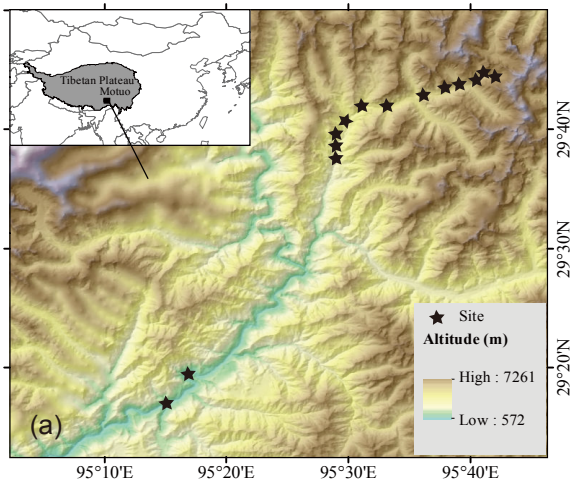
Tibetan Plateau
Motuo
Site
Altitude (m)
High : 7261
Low : 572
(a)
95°10'E
95°20'E
95°30'E
95°40'E
29°40'N
29°30'N
29°20'N

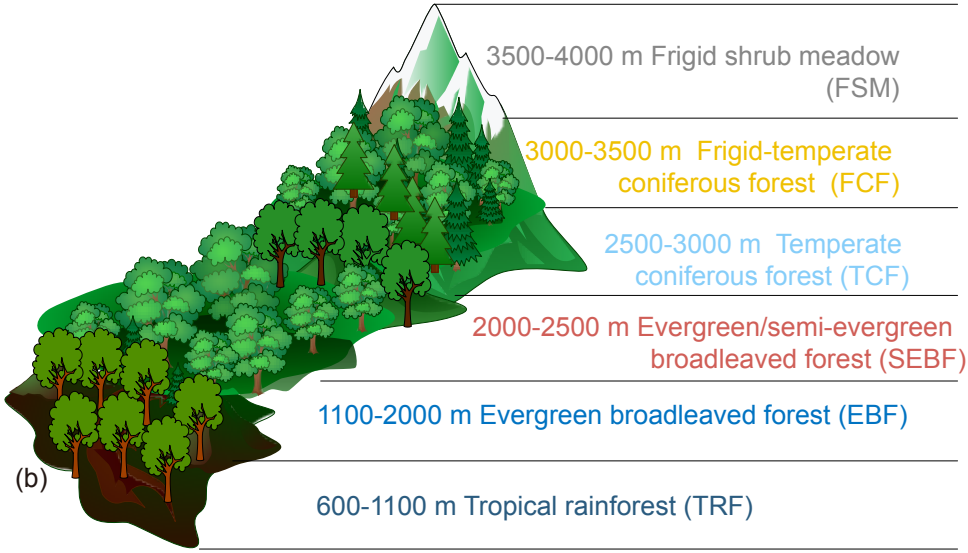
(b)
3500-4000 m Frigid shrub meadow (FSM)
3000-3500 m Frigid-temperate coniferous forest (FCF)
2500-3000 m Temperate coniferous forest (TCF)
2000-2500 m Evergreen/semi-evergreen broadleaved forest (SEBF)
1100-2000 m Evergreen broadleaved forest (EBF)
600-1100 m Tropical rainforest (TRF)

Figure 2

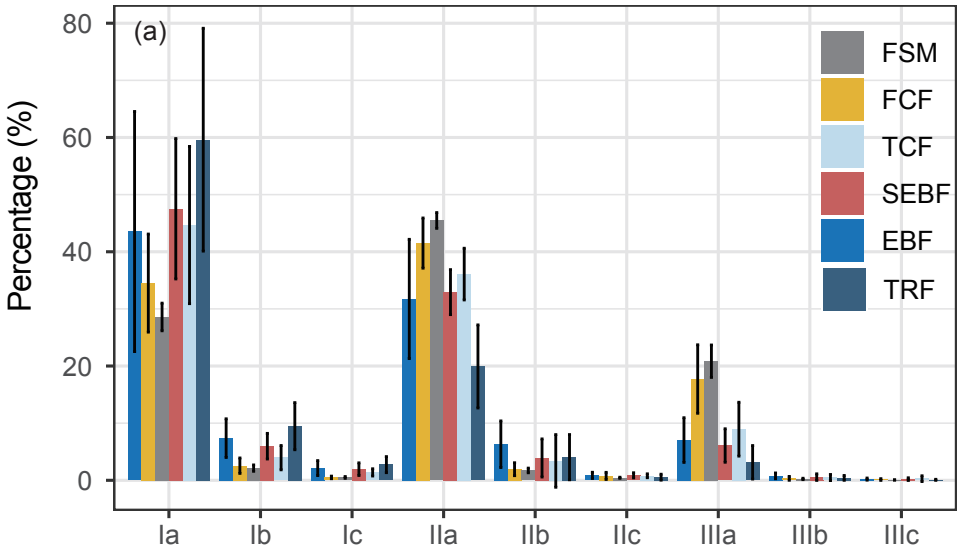
(a)
Percentage (%)
80
60
40
20
0
Ia
Ib
Ic
IIa
IIb
IIc
IIIa
IIIb
IIIc
FSM
FCF
TCF
SEBF
EBF
TRF

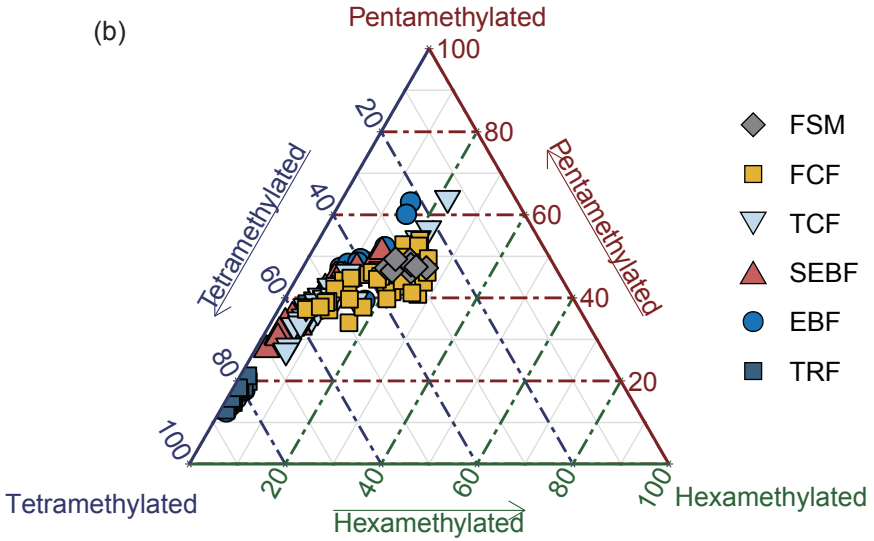
(b)
Pentamethylated
Tetramethylated
Hexamethylated
100
80
60
40
20
FSM
FCF
TCF
SEBF
EBF
TRF

Figure 3

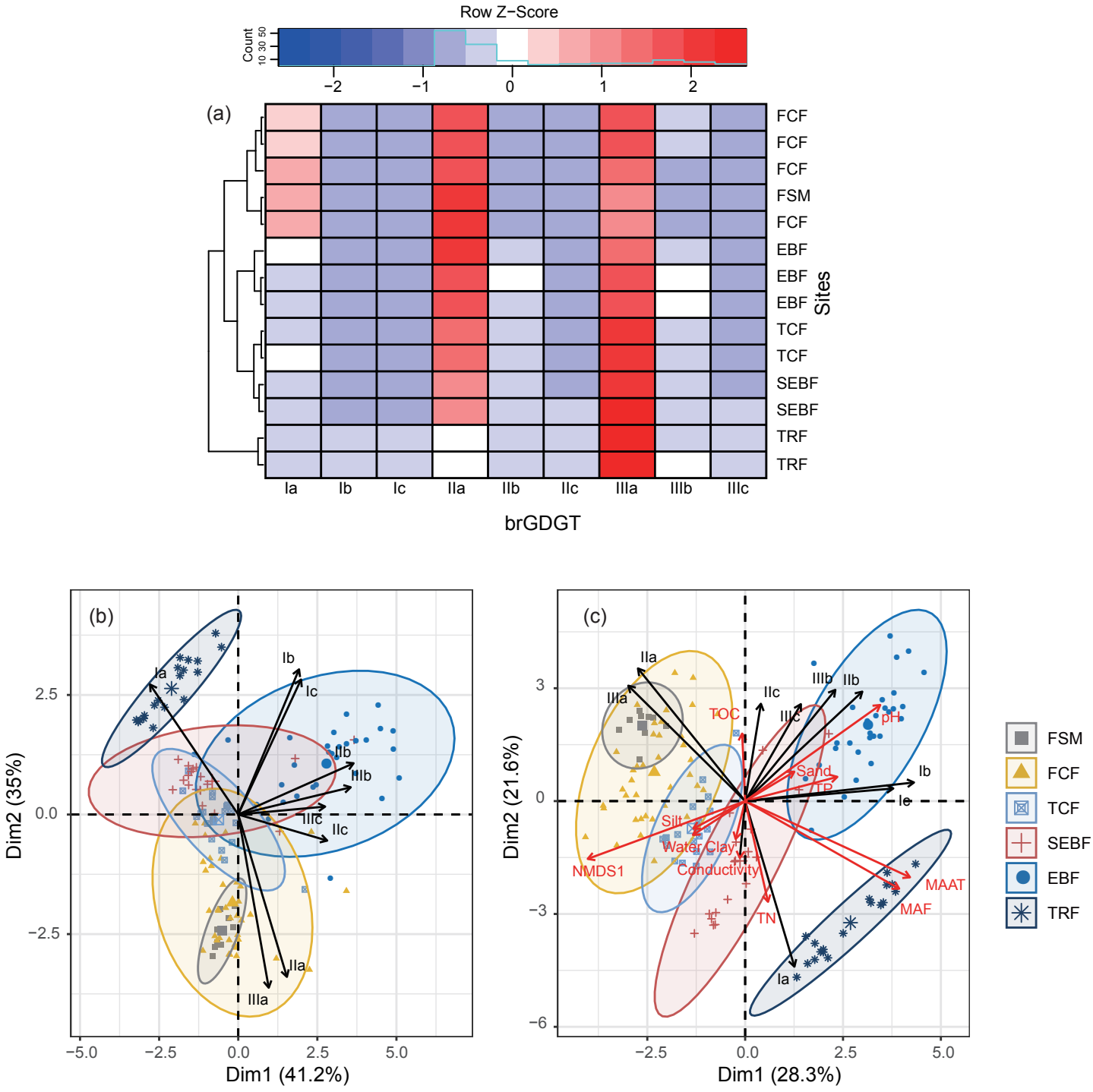
Row Z-Score
Count
10 30 50
−2
−1
0
1
2
(a)
FCF
FCF
FCF
FSM
FCF
EBF
EBF
EBF
TCF
TCF
SEBF
SEBF
TRF
TRF
Sites
Ia
Ib
Ic
IIa
IIb
IIc
IIIa
IIIb
IIIc
brGDGT
(b)
Dim2 (35%)
Dim1 (41.2%)
(c)
Dim2 (21.6%)
Dim1 (28.3%)
TOC
pH
Sand
TP
Silt
Water Clay
Conductivity
TN
NMDS1
MAAT
MAF
FSM
FCF
TCF
SEBF
EBF
TRF

Figure 4

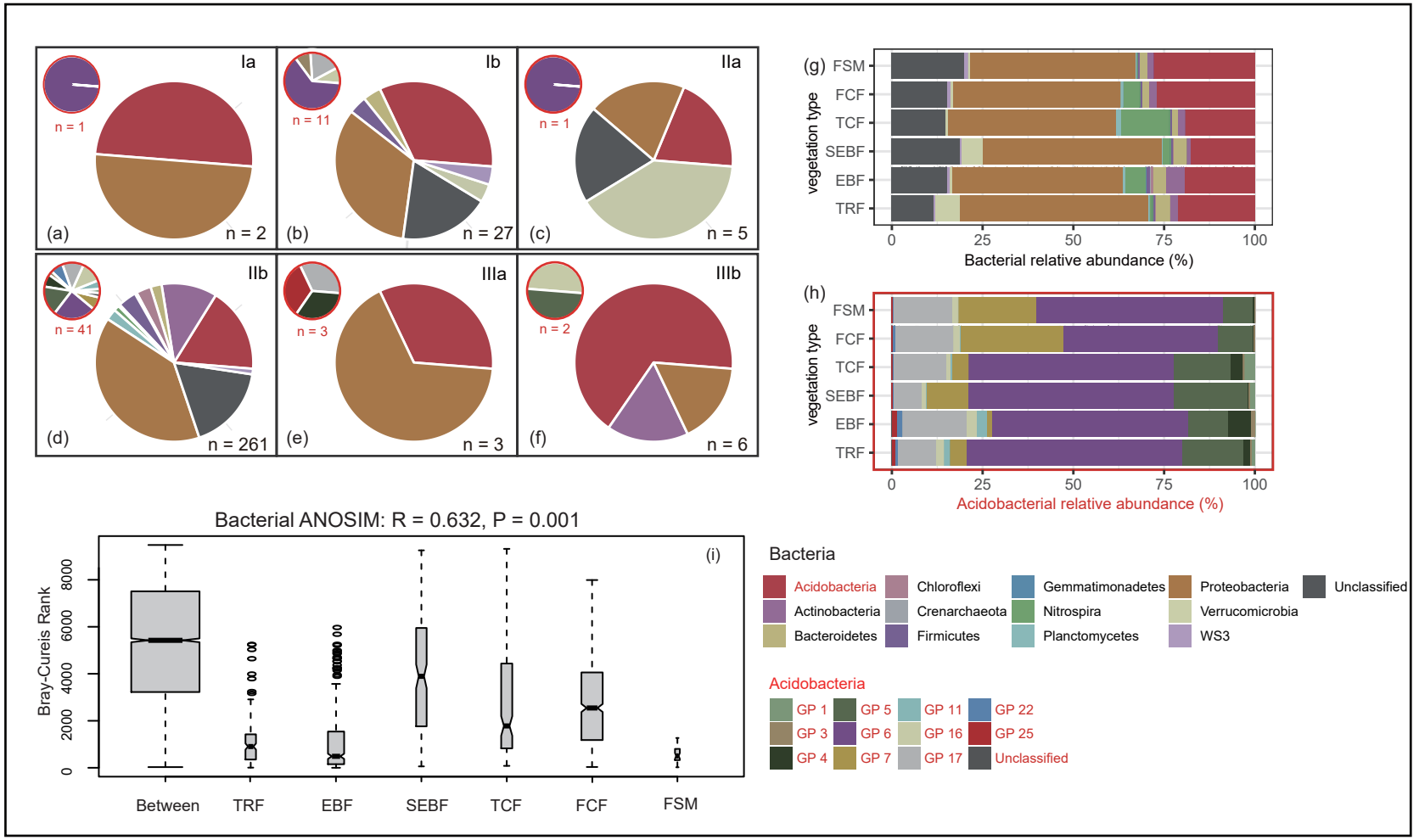
Ia
n = 1
n = 2
(a)
Ib
n = 11
n = 27
(b)
IIa
n = 1
n = 5
(c)
IIb
n = 41
n = 261
(d)
IIIa
n = 3
n = 3
(e)
IIIb
n = 2
n = 6
(f)
(g)
vegetation type
FSM
FCF
TCF
SEBF
EBF
TRF
0
25
50
75
100
Bacterial relative abundance (%)
(h)
Acidobacterial relative abundance (%)
Bacterial ANOSIM: R = 0.632, P = 0.001
(i)
Bray-Cureis Rank
0
2000
4000
6000
8000
Between
TRF
EBF
SEBF
TCF
FCF
FSM
Bacteria
Acidobacteria
Actinobacteria
Bacteroidetes
Chloroflexi
Crenarchaeota
Firmicutes
Gemmatimonadetes
Nitrospira
Planctomycetes
Proteobacteria
Verrucomicrobia
WS3
Unclassified
Acidobacteria
GP 1
GP 3
GP 4
GP 5
GP 6
GP 7
GP 11
GP 16
GP 17
GP 22
GP 25
Unclassified

Figure 5

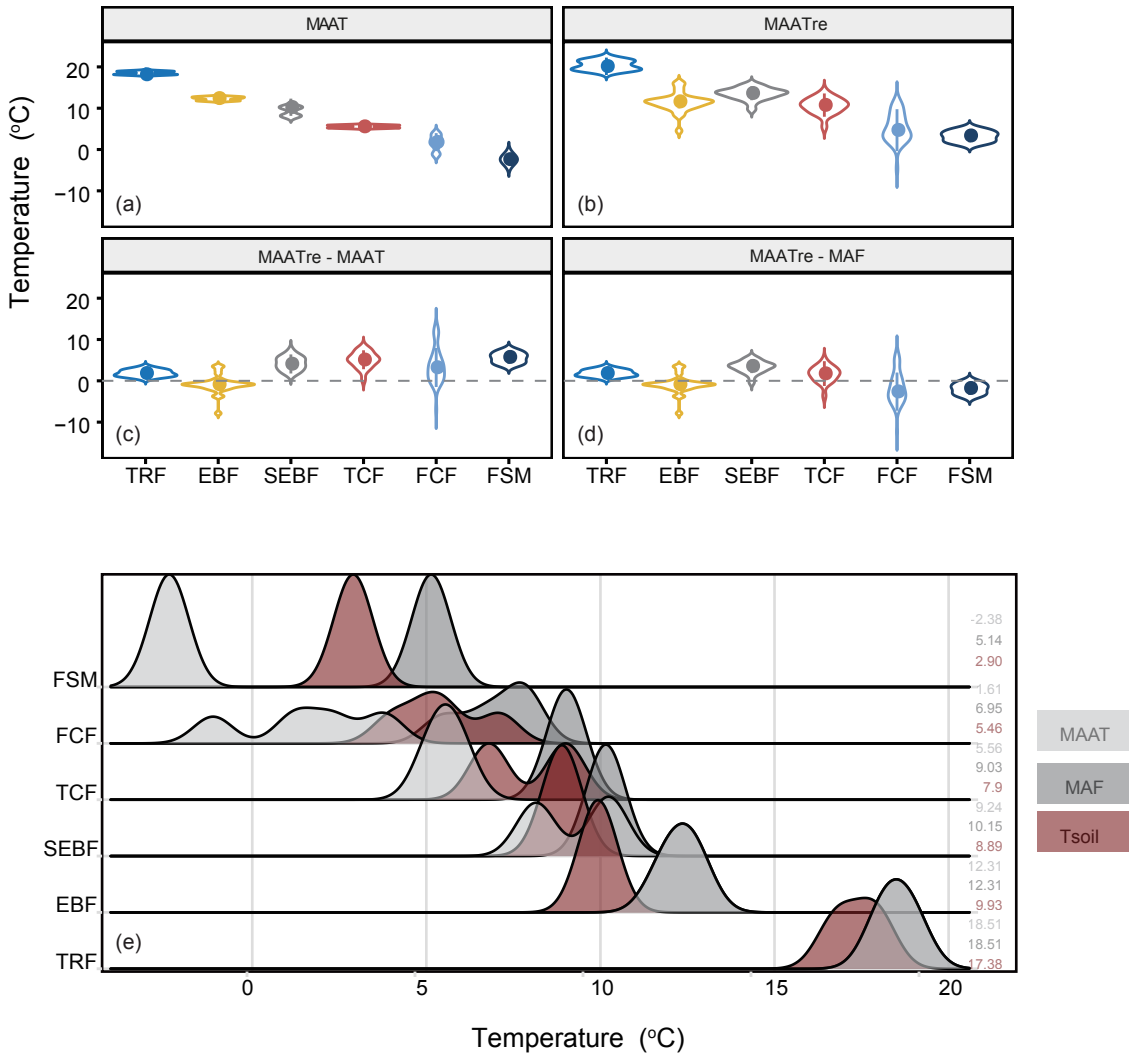
MAAT
MAATre
MAATre - MAAT
MAATre - MAF
Temperature (°C)
20
10
0
−10
(a)
(b)
(c)
(d)
TRF
EBF
SEBF
TCF
FCF
FSM
(e)
Temperature (°C)
0
5
10
15
20
MAAT
MAF
Tsoil

Figure 6

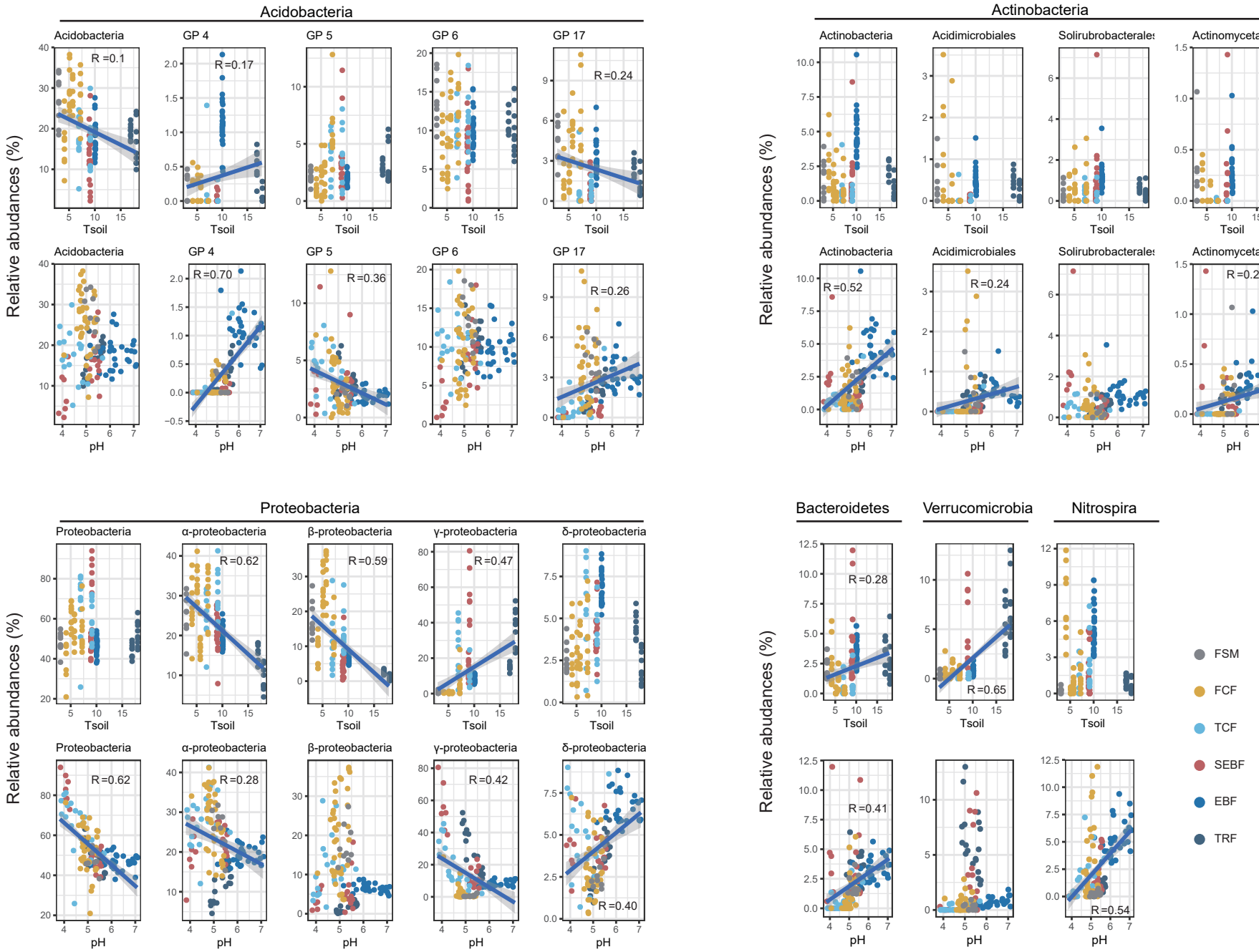
Acidobacteria
Actinobacteria
Proteobacteria
Bacteroidetes
Verrucomicrobia
Nitrospira
Relative abudances (%)
Tsoil
pH
R =0.1
R =0.17
R =0.24
R =0.70
R =0.36
R =0.26
R =0.52
R =0.24
R =0.22
R =0.62
R =0.28
R =0.59
R =0.47
R =0.42
R =0.40
R =0.28
R =0.65
R =0.41
R =0.54
FSM
FCF
TCF
SEBF
EBF
TRF

Figure 7

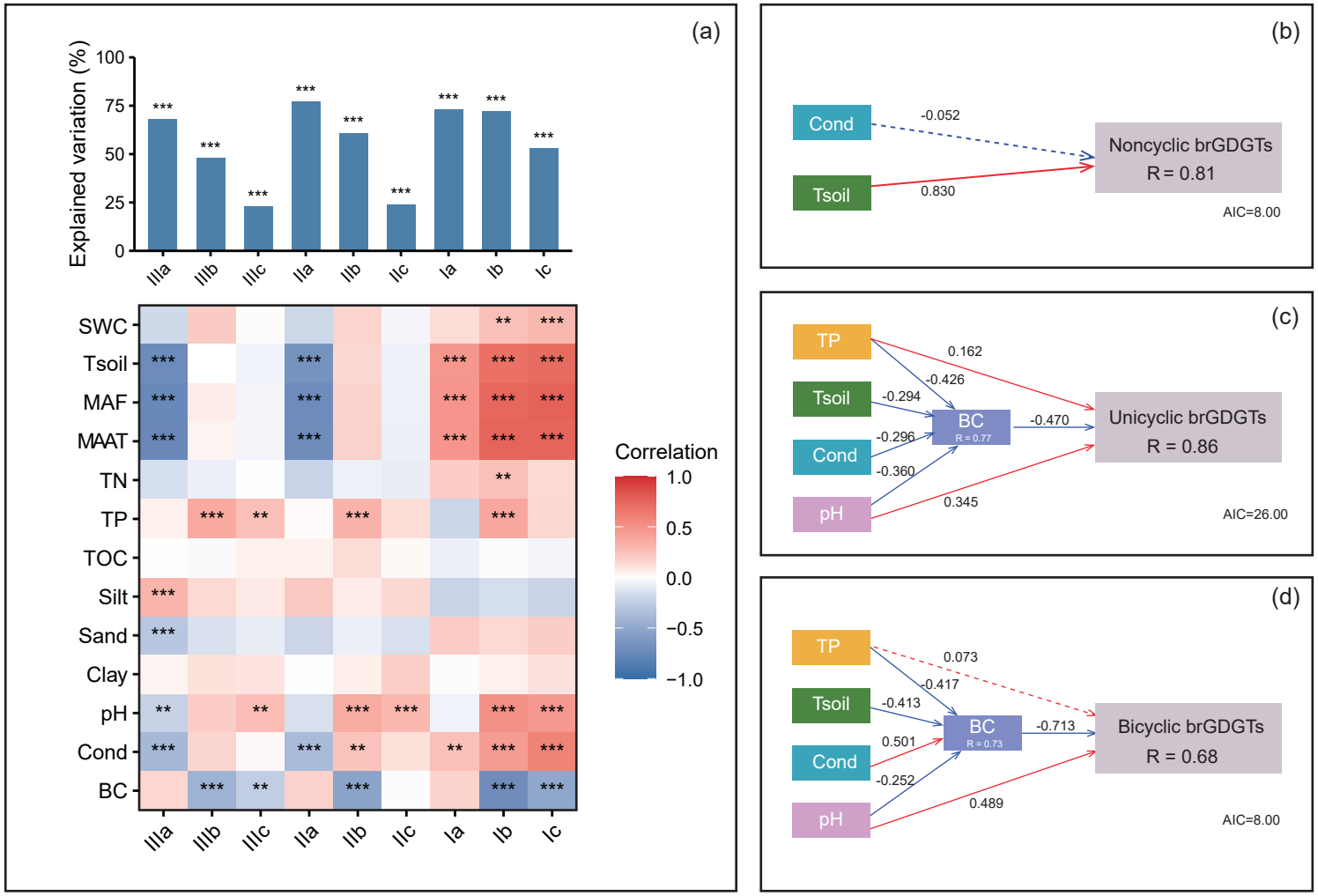
(a)
Explained variation (%)
100
75
50
25
0
IIIa
IIIb
IIIc
IIa
IIb
IIc
Ia
Ib
Ic
SWC
Tsoil
MAF
MAAT
TN
TP
TOC
Silt
Sand
Clay
pH
Cond
BC
Correlation
1.0
0.5
0.0
−0.5
−1.0
(b)
Cond
Tsoil
-0.052
0.830
Noncyclic brGDGTs
R = 0.81
AIC=8.00
(c)
TP
Tsoil
Cond
pH
0.162
-0.426
-0.294
-0.296
-0.360
0.345
BC
R = 0.77
-0.470
Unicyclic brGDGTs
R = 0.86
AIC=26.00
(d)
TP
Tsoil
Cond
pH
0.073
-0.417
-0.413
0.501
-0.252
0.489
BC
R = 0.73
-0.713
Bicyclic brGDGTs
R = 0.68
AIC=8.00

Figure 8

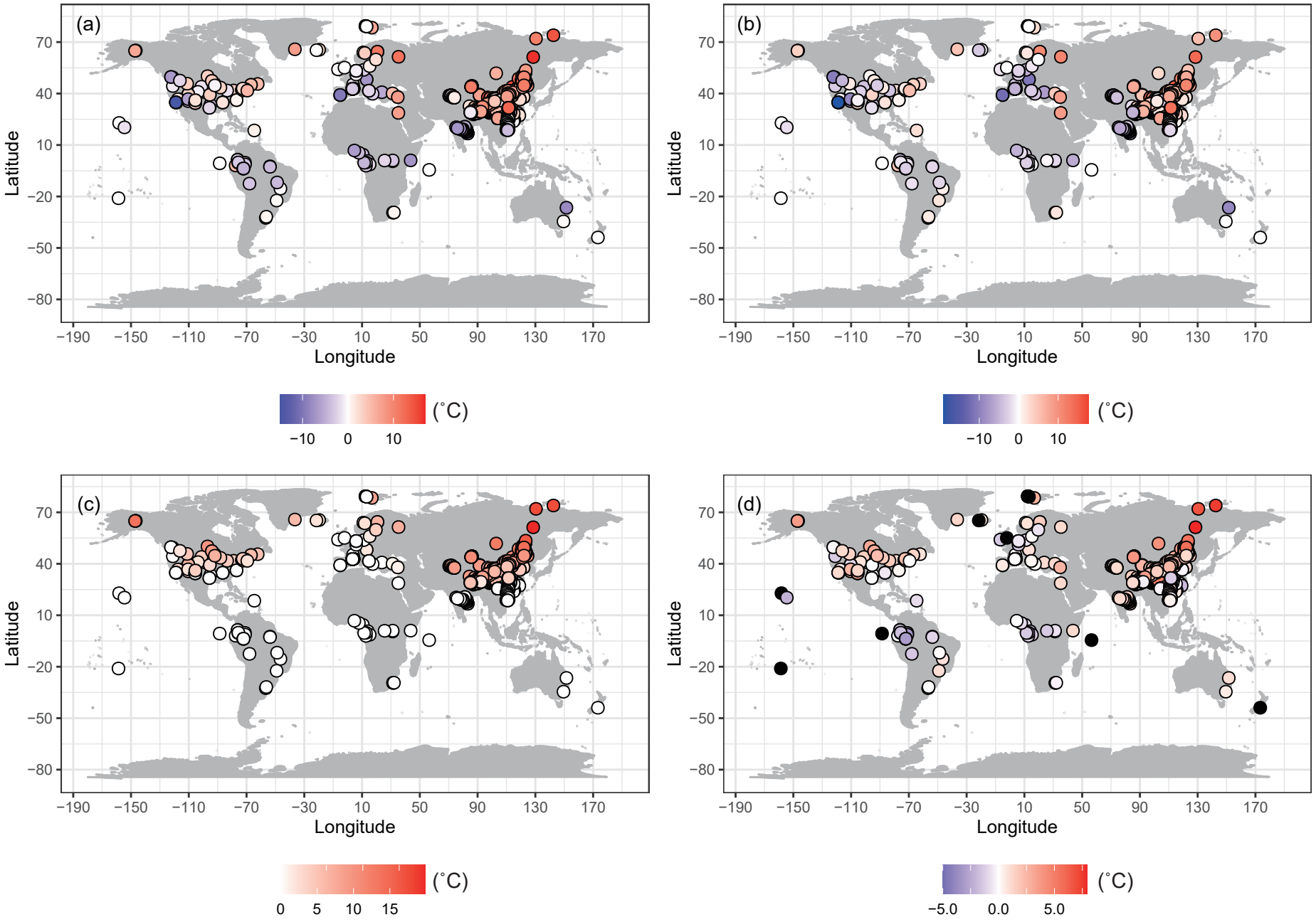
(a)
(b)
(c)
(d)
Latitude
Longitude
70
40
10
−20
−50
−80
−190
−150
−110
−70
−30
10
50
90
130
170
(˚C)
−10
0
10
0
5
10
15
−5.0
0.0
5.0

Supplementary Information for

Branched glycerol dialkyl glycerol tetraether (brGDGT) distributions influenced by bacterial community composition in various vegetation soils on the Tibetan Plateau

Jie Liang, Nora Richter, Haichao Xie, Boyang Zhao, Guicai Si, Jian Wang, Juzhi Hou*, Gengxin Zhang *, James M. Russell

*** To whom correspondence should be addressed. Email:**
Gengxin Zhang, zhangg@itpcas.ac.cn
Juzhi Hou, houjz@itpcas.ac.cn

This PDF file includes:

Figure S1

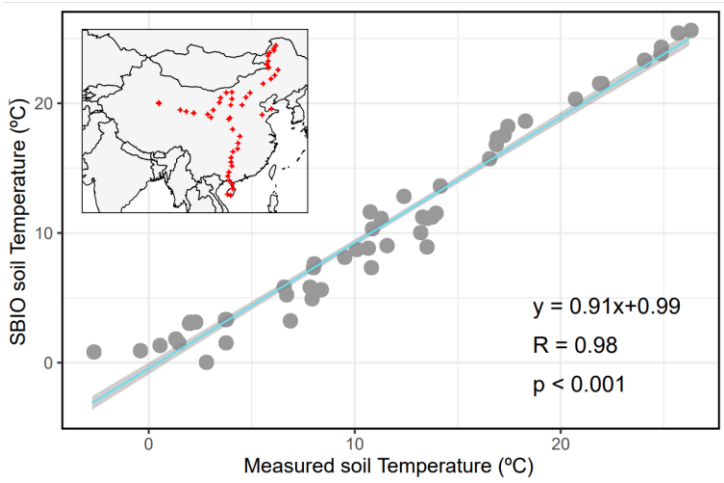

Figure S1. Linear regression of mean annual soil temperature (Wang et al., 2020) vs. SBIO global mean annual soil temperature (Lembrechts et al., 2022). The red dots in the map indicate the locations of the in situ soil temperature measurements (Wang et al. 2020).

Figure S2

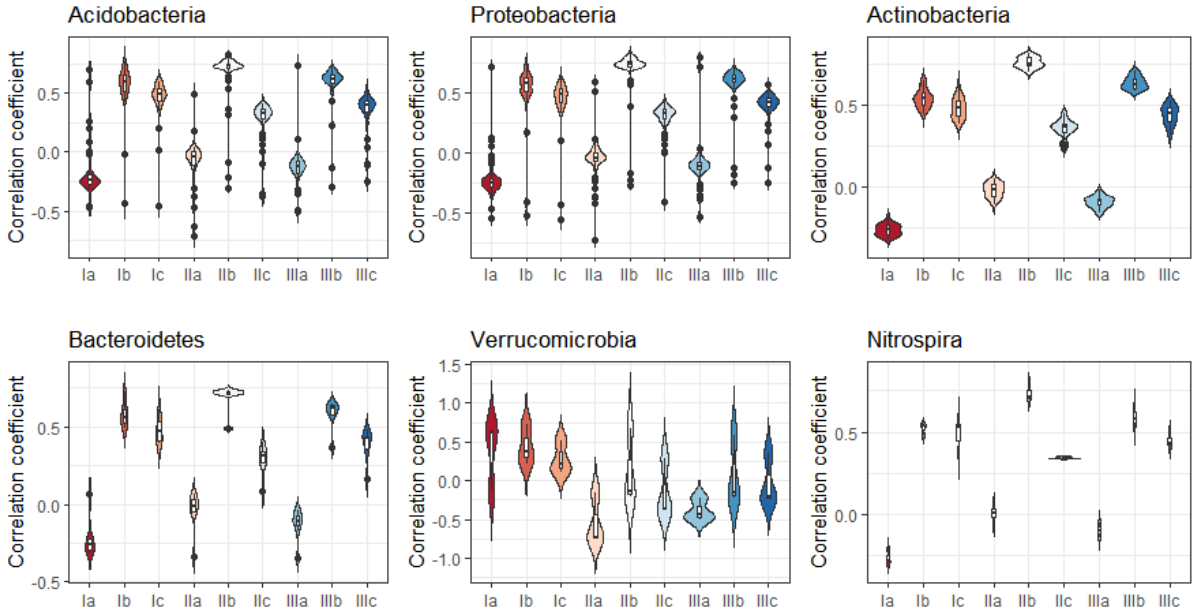

Figure S2. Violin plots of Pearson correlation coefficients between bacteria and brGDGTs compounds.

Dataset S1 Geographical and environmental data for our study sites, including elevation, latitude, longitude, vegetation type, mean annual air temperature (MAAT), mean temperature of months above freezing (MAF), mean annual soil temperature (Tsoil), water content (WC), conductivity, pH, TOC, TN, TP, sand, silt, and clay.

SampleID	Elevation (m)	Lat (°)	Long (°)	Vegetation	MAAT (°)	MAF (°)	Tsoil (°)	WC (%)	Conductivity (us cm-1)	pH	TOC (%)	TN (mg/kg)	TP (mg/kg)	Sand (%)	Silt (%)	Clay (%)
MT02_01	704	29.28	95.26	TRF	18.92	18.92	16.80	5.93	29.40	6	1.60	2.80	2.05	74.68	25.32	0.00
MT02_02	704	29.28	95.26	TRF	18.92	18.92	16.80	6.13	24.20	6	1.60	3.29	2.10	76.99	23.01	0.00
MT02_03	704	29.28	95.26	TRF	18.92	18.92	16.80	7.90	37.40	5	1.70	4.91	2.03	76.66	22.01	1.33
MT02_05	704	29.28	95.26	TRF	18.92	18.92	16.80	6.37	30.70	6	1.50	3.95	1.45	78.05	21.23	0.72
MT02_06	704	29.28	95.26	TRF	18.92	18.92	16.80	6.11	31.80	6	1.70	6.82	2.29	74.20	24.50	1.30
MT02_07	704	29.28	95.26	TRF	18.92	18.92	16.80	5.13	35.30	6	2.00	5.06	2.16	77.50	21.80	0.70
MT02_08	704	29.28	95.26	TRF	18.92	18.92	16.80	10.79	44.50	6	1.70	5.60	2.38	71.83	28.17	0.00
MT02_09	704	29.28	95.26	TRF	18.92	18.92	16.80	8.49	59.50	6	1.50	7.31	2.24	59.26	39.95	0.79
MT02_10	704	29.28	95.26	TRF	18.92	18.92	16.80	7.20	30.40	6	1.50	4.74	1.93	67.34	31.85	0.82
MT04_01	877	29.32	95.29	TRF	18.15	18.15	17.90	15.45	65.70	5	1.40	10.48	4.00	53.42	44.53	2.05
MT04_02	877	29.32	95.29	TRF	18.15	18.15	17.90	16.19	59.00	5	1.60	9.78	3.76	47.34	50.22	2.44
MT04_03	877	29.32	95.29	TRF	18.15	18.15	17.90	14.69	54.40	5	1.50	9.86	3.81	54.09	43.74	2.17
MT04_04	877	29.32	95.29	TRF	18.15	18.15	17.90	13.62	49.70	5	1.50	9.82	3.69	40.28	55.39	4.33
MT04_05	877	29.32	95.29	TRF	18.15	18.15	17.90	14.92	52.90	5	1.50	9.86	3.43	53.05	46.10	0.85
MT04_06	877	29.32	95.29	TRF	18.15	18.15	17.90	15.32	55.10	5	1.80	10.00	3.62	39.72	57.77	2.51
MT04_07	877	29.32	95.29	TRF	18.15	18.15	17.90	19.73	62.00	5	1.40	10.80	4.04	49.50	48.61	1.89
MT04_08	877	29.32	95.29	TRF	18.15	18.15	17.90	14.95	43.80	5	1.40	9.43	3.28	56.51	41.96	1.53
MT04_09	877	29.32	95.29	TRF	18.15	18.15	17.90	13.08	39.40	5	1.30	9.20	3.35	46.58	50.85	2.57
MT04_10	877	29.32	95.29	TRF	18.15	18.15	17.90	12.50	31.60	5	1.60	8.23	3.06	56.11	41.95	1.95
MT05_01	1893	29.64	95.49	EBF	11.80	11.80	9.90	12.44	54.30	6	1.40	5.26	4.33	63.82	36.18	0.00
MT05_02	1893	29.64	95.49	EBF	11.80	11.80	9.90	17.72	57.90	6	1.50	6.67	4.04	73.93	26.07	0.00
MT05_03	1893	29.64	95.49	EBF	11.80	11.80	9.90	22.56	49.30	6	1.70	8.34	4.53	73.94	25.63	0.43
MT05_04	1893	29.64	95.49	EBF	11.80	11.80	9.90	10.24	29.60	6	1.80	4.69	4.50	61.09	38.17	0.74
MT05_05	1893	29.64	95.49	EBF	11.80	11.80	9.90	7.04	28.10	6	1.70	2.69	3.63	71.19	28.43	0.38
MT05_06	1893	29.64	95.49	EBF	11.80	11.80	9.90	32.53	65.40	5	1.40	8.36	3.53	75.31	24.24	0.45
MT05_07	1893	29.64	95.49	EBF	11.80	11.80	9.90	11.74	39.30	6	1.80	3.77	4.86	57.27	42.73	0.00

SampleID	Elevation (m)	Lat (°)	Long (°)	Vegetation	MAAT (°)	MAF (°)	Tsoil (°)	WC (%)	Conductivity (us cm-1)	pH	TOC (%)	TN （mg/kg)	TP （mg/kg)	Sand (%)	Silt (%)	Clay (%)
MT05_08	1893	29.64	95.49	EBF	11.80	11.80	9.90	11.72	29.60	6	1.30	4.20	4.80	67.85	30.69	1.46
MT05_09	1893	29.64	95.49	EBF	11.80	11.80	9.90	19.59	71.10	6	1.40	6.59	4.38	70.88	28.43	0.69
MT05_10	1893	29.64	95.49	EBF	11.80	11.80	9.90	11.92	49.50	6	1.80	5.98	3.76	68.69	30.34	0.97
MT06_01	1669	29.63	95.49	EBF	12.39	12.39	10.00	13.49	73.30	7	2.10	4.18	3.00	70.14	28.62	1.24
MT06_02	1669	29.63	95.49	EBF	12.39	12.39	10.00	7.71	27.50	7	1.80	1.45	3.20	71.04	27.52	1.44
MT06_03	1669	29.63	95.49	EBF	12.39	12.39	10.00	8.51	27.80	7	1.80	2.42	2.68	70.49	27.96	1.56
MT06_05	1669	29.63	95.49	EBF	12.39	12.39	10.00	7.69	33.10	7	1.90	2.26	2.81	67.06	30.70	2.24
MT06_06	1669	29.63	95.49	EBF	12.39	12.39	10.00	9.32	39.60	7	1.70	2.82	2.79	68.91	29.65	1.44
MT06_07	1669	29.63	95.49	EBF	12.39	12.39	10.00	16.77	71.50	7	2.10	3.68	2.68	61.51	36.97	1.51
MT06_08	1669	29.63	95.49	EBF	12.39	12.39	10.00	10.26	36.30	7	1.80	3.59	2.72	63.84	34.15	2.01
MT06_09	1669	29.63	95.49	EBF	12.39	12.39	10.00	15.20	73.00	7	1.50	3.71	2.96	54.29	43.65	2.06
MT06_10	1669	29.63	95.49	EBF	12.39	12.39	10.00	10.22	28.90	7	1.40	2.30	3.37	69.96	28.62	1.41
MT07_01	1546	29.61	95.49	EBF	12.76	12.76	9.90	24.39	65.70	6	1.40	8.97	2.67	58.55	38.76	2.69
MT07_02	1546	29.61	95.49	EBF	12.76	12.76	9.90	37.38	98.10	6	1.50	12.07	2.86	57.49	40.43	2.08
MT07_03	1546	29.61	95.49	EBF	12.76	12.76	9.90	22.40	88.20	6	1.60	8.19	2.70	59.31	39.13	1.55
MT07_04	1546	29.61	95.49	EBF	12.76	12.76	9.90	20.55	77.80	6	1.40	5.37	2.91	35.00	59.61	5.39
MT07_05	1546	29.61	95.49	EBF	12.76	12.76	9.90	40.52	115.50	6	1.60	12.18	3.16	66.89	31.63	1.49
MT07_06	1546	29.61	95.49	EBF	12.76	12.76	9.90	14.81	48.90	6	2.10	4.06	3.00	60.85	36.01	3.13
MT07_07	1546	29.61	95.49	EBF	12.76	12.76	9.90	19.25	57.50	6	1.40	6.12	2.89	56.45	41.27	2.28
MT07_08	1546	29.61	95.49	EBF	12.76	12.76	9.90	6.51	28.50	6	1.90	3.72	2.73	74.88	23.72	1.40
MT07_09	1546	29.61	95.49	EBF	12.76	12.76	9.90	76.61	167.30	6	1.50	14.05	2.62	52.28	45.46	2.25
MT07_10	1546	29.61	95.49	EBF	12.76	12.76	9.90	11.11	42.80	6	1.50	4.46	3.17	56.65	40.59	2.76
MT08_01	2166	29.67	95.50	SEBF	10.23	10.23	8.80	13.15	35.30	5	1.50	4.25	1.84	64.48	33.94	1.58
MT08_02	2166	29.67	95.50	SEBF	10.23	10.23	8.80	13.16	33.30	5	1.60	5.83	2.09	70.15	29.53	0.32
MT08_03	2166	29.67	95.50	SEBF	10.23	10.23	8.80	28.47	49.60	5	1.30	7.32	2.52	64.70	33.09	2.21
MT08_04	2166	29.67	95.50	SEBF	10.23	10.23	8.80	14.35	23.90	6	1.90	5.48	2.28	51.21	45.15	3.64
MT08_05	2166	29.67	95.50	SEBF	10.23	10.23	8.80	23.78	53.30	5	1.60	6.34	1.91	61.95	35.70	2.35
MT08_06	2166	29.67	95.50	SEBF	10.23	10.23	8.80	21.15	38.10	5	1.30	6.80	2.32	42.00	53.75	4.25
MT08_07	2166	29.67	95.50	SEBF	10.23	10.23	8.80	15.03	22.50	6	1.50	3.41	1.64	43.95	51.75	4.30
MT08_08	2166	29.67	95.50	SEBF	10.23	10.23	8.80	24.08	29.80	5	1.30	6.86	2.96	48.19	48.27	3.54

SampleID	Elevation (m)	Lat (°)	Long (°)	Vegetation	MAAT (°)	MAF (°)	Tsoil (°)	WC (%)	Conductivity (us cm-1)	pH	TOC (%)	TN （mg/kg)	TP （mg/kg)	Sand (%)	Silt (%)	Clay (%)
MT08_09	2166	29.67	95.50	SEBF	10.23	10.23	8.80	22.17	26.90	5	1.50	5.98	2.33	53.30	43.14	3.56
MT08_10	2166	29.67	95.50	SEBF	10.23	10.23	8.80	25.12	45.80	5	1.50	6.47	2.12	48.08	48.27	3.65
MT09_01	2438	29.70	95.52	SEBF	8.15	10.07	9.00	6.31	48.70	6	1.60	7.21	1.24	71.61	27.90	0.50
MT09_02	2438	29.70	95.52	SEBF	8.15	10.07	9.00	9.15	27.00	5	1.80	8.05	1.12	73.41	25.97	0.62
MT09_04	2438	29.70	95.52	SEBF	8.15	10.07	9.00	28.20	101.80	4	1.60	11.51	1.49	74.17	24.82	1.01
MT09_05	2438	29.70	95.52	SEBF	8.15	10.07	9.00	37.67	176.50	4	1.30	14.01	1.98	64.56	34.16	1.28
MT09_06	2438	29.70	95.52	SEBF	8.15	10.07	9.00	26.30	146.10	4	1.60	12.84	1.77	80.90	18.68	0.42
MT09_07	2438	29.70	95.52	SEBF	8.15	10.07	9.00	46.67	179.50	4	1.40	15.18	2.67	71.86	27.05	1.09
MT09_08	2438	29.70	95.52	SEBF	8.15	10.07	9.00	35.79	209.00	4	1.30	15.26	2.20	67.61	32.06	0.33
MT09_09	2438	29.70	95.52	SEBF	8.15	10.07	9.00	29.69	166.30	4	1.60	14.06	2.13	65.66	33.20	1.14
MT09_10	2438	29.70	95.52	SEBF	8.15	10.07	9.00	35.02	164.50	4	1.40	14.49	2.22	58.62	40.67	0.70
MT12_01	2743	29.70	95.56	TCF	5.88	8.91	9.00	11.88	25.00	5	1.70	2.88	1.42	71.70	28.30	0.00
MT12_02	2743	29.70	95.56	TCF	5.88	8.91	9.00	13.63	36.10	5	1.50	6.02	2.05	73.59	25.75	0.66
MT12_03	2743	29.70	95.56	TCF	5.88	8.91	9.00	13.62	28.40	5	1.80	4.63	1.79	65.11	33.77	1.12
MT12_04	2743	29.70	95.56	TCF	5.88	8.91	9.00	16.38	36.80	5	1.50	5.08	1.72	64.03	34.49	1.47
MT12_05	2743	29.70	95.56	TCF	5.88	8.91	9.00	18.04	54.20	5	2.00	7.07	2.06	65.82	32.65	1.54
MT12_06	2743	29.70	95.56	TCF	5.88	8.91	9.00	17.72	41.80	5	1.30	4.89	1.61	60.52	37.62	1.86
MT12_07	2743	29.70	95.56	TCF	5.88	8.91	9.00	17.51	52.90	4	1.40	6.92	1.93	68.94	29.60	1.46
MT12_08	2743	29.70	95.56	TCF	5.88	8.91	9.00	17.48	51.20	4	1.40	7.54	1.84	70.94	27.84	1.22
MT12_09	2743	29.70	95.56	TCF	5.88	8.91	9.00	14.11	34.10	5	1.40	4.27	1.80	58.89	38.97	2.14
MT12_10	2743	29.70	95.56	TCF	5.88	8.91	9.00	14.67	37.10	5	1.70	5.60	1.73	69.03	29.90	1.07
MT13_01	2964	29.72	95.61	TCF	5.23	9.14	6.80	64.74	115.00	6	1.60	8.97	2.34	66.06	31.45	2.49
MT13_02	2964	29.72	95.61	TCF	5.23	9.14	6.80	17.92	46.00	4	1.40	3.09	0.96	72.07	25.92	2.00
MT13_03	2964	29.72	95.61	TCF	5.23	9.14	6.80	27.88	72.50	4	1.50	4.33	0.86	50.47	46.72	2.81
MT13_04	2964	29.72	95.61	TCF	5.23	9.14	6.80	21.00	55.10	4	1.40	2.67	0.87	78.14	21.86	0.00
MT13_05	2964	29.72	95.61	TCF	5.23	9.14	6.80	22.11	59.20	4	1.60	4.19	0.97	46.02	50.70	3.28
MT13_06	2964	29.72	95.61	TCF	5.23	9.14	6.80	23.37	52.40	4	1.50	2.61	0.83	47.63	49.18	3.19
MT13_07	2964	29.72	95.61	TCF	5.23	9.14	6.80	16.41	39.20	4	1.60	2.76	0.79	43.59	53.16	3.25
MT13_08	2964	29.72	95.61	TCF	5.23	9.14	6.80	20.06	47.80	4	1.40	3.60	1.01	53.23	44.13	2.64
MT13_09	2964	29.72	95.61	TCF	5.23	9.14	6.80	28.66	70.10	4	1.50	6.47	1.23	61.07	36.79	2.14

SampleID	Elevation (m)	Lat (°)	Long (°)	Vegetation	MAAT (°)	MAF (°)	Tsoil (°)	WC (%)	Conductivity (us cm-1)	pH	TOC (%)	TN （mg/kg)	TP （mg/kg)	Sand (%)	Silt (%)	Clay (%)
MT13_10	2964	29.72	95.61	TCF	5.23	9.14	6.80	34.09	90.40	4	1.70	4.30	0.87	59.92	38.00	2.07
MT14_01	3144	29.72	95.64	FCF	3.78	7.89	7.10	43.33	68.60	5	1.50	7.95	2.30	86.74	12.86	0.40
MT14_02	3144	29.72	95.64	FCF	3.78	7.89	7.10	29.00	65.50	5	1.70	6.59	1.96	33.76	62.82	3.41
MT14_03	3144	29.72	95.64	FCF	3.78	7.89	7.10	20.50	58.60	5	1.50	4.81	1.68	68.80	30.39	0.81
MT14_04	3144	29.72	95.64	FCF	3.78	7.89	7.10	16.74	40.30	5	1.90	2.23	1.09	44.80	52.73	2.47
MT14_05	3144	29.72	95.64	FCF	3.78	7.89	7.10	29.48	59.00	5	1.40	8.96	2.42	45.35	52.29	2.35
MT14_06	3144	29.72	95.64	FCF	3.78	7.89	7.10	27.87	45.80	5	1.50	5.96	1.95	58.25	40.02	1.74
MT14_07	3144	29.72	95.64	FCF	3.78	7.89	7.10	24.57	54.40	5	1.70	4.59	1.62	58.28	39.95	1.77
MT14_08	3144	29.72	95.64	FCF	3.78	7.89	7.10	22.16	45.10	5	1.70	3.27	1.36	40.19	56.35	3.46
MT14_09	3144	29.72	95.64	FCF	3.78	7.89	7.10	39.58	65.70	5	1.50	8.98	2.40	57.77	40.33	1.89
MT14_10	3144	29.72	95.64	FCF	3.78	7.89	7.10	20.87	87.40	4	1.50	4.68	1.32	64.96	32.76	2.28
MT15_01	3244	29.73	95.66	FCF	2.33	7.70	5.60	7.01	31.10	5	2.00	0.73	2.68	54.83	45.17	0.00
MT15_02	3244	29.73	95.66	FCF	2.33	7.70	5.60	4.06	20.30	5	1.90	0.58	2.79	65.10	34.90	0.00
MT15_03	3244	29.73	95.66	FCF	2.33	7.70	5.60	4.33	19.77	5	1.50	0.59	3.00	69.81	29.69	0.51
MT15_04	3244	29.73	95.66	FCF	2.33	7.70	5.60	12.13	37.50	5	1.30	2.64	1.28	44.64	52.85	2.52
MT15_05	3244	29.73	95.66	FCF	2.33	7.70	5.60	4.87	26.10	5	1.80	1.01	2.60	57.96	42.05	0.00
MT15_06	3244	29.73	95.66	FCF	2.33	7.70	5.60	5.01	27.40	5	2.00	0.65	2.88	66.05	33.95	0.00
MT15_07	3244	29.73	95.66	FCF	2.33	7.70	5.60	3.63	26.00	5	1.70	0.45	2.74	69.63	30.37	0.00
MT15_09	3244	29.73	95.66	FCF	2.33	7.70	5.60	4.81	20.90	5	2.00	0.57	2.85	71.58	28.42	0.00
MT15_10	3244	29.73	95.66	FCF	2.33	7.70	5.60	5.65	23.00	5	1.60	0.71	2.89	67.18	32.82	0.00
MT16_01	3419	29.74	95.68	FCF	1.24	6.70	5.00	37.82	67.40	5	1.70	6.29	2.45	36.00	60.54	3.45
MT16_02	3419	29.74	95.68	FCF	1.24	6.70	5.00	86.77	91.70	5	1.70	10.78	2.76	28.19	66.86	4.96
MT16_03	3419	29.74	95.68	FCF	1.24	6.70	5.00	40.76	59.80	5	1.80	8.30	2.10	58.84	39.34	1.82
MT16_04	3419	29.74	95.68	FCF	1.24	6.70	5.00	41.88	49.70	5	1.40	6.74	1.91	40.77	55.77	3.46
MT16_05	3419	29.74	95.68	FCF	1.24	6.70	5.00	38.93	51.60	5	1.40	7.61	2.14	44.72	52.84	2.44
MT16_06	3419	29.74	95.68	FCF	1.24	6.70	5.00	32.47	45.40	5	2.00	4.30	1.57	51.06	46.77	2.16
MT16_07	3419	29.74	95.68	FCF	1.24	6.70	5.00	67.05	75.60	5	1.30	10.35	2.26	50.43	47.15	2.42
MT16_08	3419	29.74	95.68	FCF	1.24	6.70	5.00	34.81	61.30	5	1.60	5.14	1.67	59.94	37.47	2.59
MT16_09	3419	29.74	95.68	FCF	1.24	6.70	5.00	26.61	48.30	5	1.80	4.63	1.51	61.32	38.68	0.00
MT16_10	3419	29.74	95.68	FCF	1.24	6.70	5.00	91.10	92.20	5	1.40	12.41	2.65	26.96	69.22	3.82

SampleID	Elevation (m)	Lat (°)	Long (°)	Vegetation	MAAT (°)	MAF (°)	Tsoil (°)	WC (%)	Conductivity (us cm-1)	pH	TOC (%)	TN （mg/kg)	TP （mg/kg)	Sand (%)	Silt (%)	Clay (%)
MT17_01	3629	29.74	95.69	FCF	-1.13	5.45	2.90	8.80	18.58	5	1.80	2.52	3.23	53.24	46.76	0.00
MT17_03	3629	29.74	95.69	FCF	-1.13	5.45	2.90	9.23	24.70	5	1.90	2.08	3.23	57.22	42.78	0.00
MT17_04	3629	29.74	95.69	FCF	-1.13	5.45	2.90	12.55	27.50	5	1.30	3.36	3.21	55.01	44.99	0.00
MT17_05	3629	29.74	95.69	FCF	-1.13	5.45	2.90	16.26	16.66	5	1.70	4.03	3.24	56.36	43.64	0.00
MT17_06	3629	29.74	95.69	FCF	-1.13	5.45	2.90	10.48	18.86	5	1.30	2.64	3.10	54.87	45.13	0.00
MT17_07	3629	29.74	95.69	FCF	-1.13	5.45	2.90	19.85	22.00	5	1.40	3.24	2.99	49.13	49.00	1.87
MT17_08	3629	29.74	95.69	FCF	-1.13	5.45	2.90	26.89	114.20	5	1.60	9.88	3.86	51.65	47.29	1.06
MT17_09	3629	29.74	95.69	FCF	-1.13	5.45	2.90	18.98	54.00	5	1.40	8.10	3.70	53.47	46.53	0.00
MT17_10	3629	29.74	95.69	FCF	-1.13	5.45	2.90	25.79	62.80	5	1.40	8.73	3.97	39.42	59.47	1.11
MT18_01	3760	29.74	95.71	FSM	-2.38	5.14	4.00	4.53	29.40	5	2.10	1.10	1.39	78.65	20.94	0.40
MT18_02	3760	29.74	95.71	FSM	-2.38	5.14	4.00	5.21	28.80	5	1.70	1.09	2.15	74.68	24.80	0.51
MT18_03	3760	29.74	95.71	FSM	-2.38	5.14	4.00	7.69	24.70	5	1.70	1.10	1.52	62.36	36.59	1.05
MT18_04	3760	29.74	95.71	FSM	-2.38	5.14	4.00	2.97	24.90	5	1.90	0.94	1.71	76.74	22.22	1.04
MT18_05	3760	29.74	95.71	FSM	-2.38	5.14	4.00	6.22	29.50	5	2.20	1.48	1.59	52.23	45.69	2.09
MT18_06	3760	29.74	95.71	FSM	-2.38	5.14	4.00	7.31	26.60	5	1.30	0.92	1.70	59.10	39.34	1.55
MT18_07	3760	29.74	95.71	FSM	-2.38	5.14	4.00	5.42	27.80	5	2.00	1.15	1.70	70.69	28.21	1.10
MT18_08	3760	29.74	95.71	FSM	-2.38	5.14	4.00	6.03	25.70	5	1.60	1.33	1.66	78.93	20.60	0.47
MT18_09	3760	29.74	95.71	FSM	-2.38	5.14	4.00	5.76	22.70	5	2.10	1.01	1.53	76.81	22.67	0.51

Dataset S2 Relative abundance of brGDGTs from this study.

Sample ID	IIIa	IIIb	IIIc	IIa	IIb	IIc	Ia	Ib	Ic
MT02_01	0.99	0.09	0.04	15.19	1.91	0.13	67.67	11.76	2.22
MT02_02	2.28	0.04	0.05	17.40	2.18	0.28	64.32	10.81	2.64
MT02_03	1.04	0.07	0.04	12.24	1.83	0.17	71.80	10.68	2.13
MT02_05	1.55	0.21	0.03	12.90	1.63	0.28	72.64	8.88	1.87
MT02_06	1.20	0.19	0.05	13.44	1.12	0.15	73.30	7.93	2.61
MT02_07	1.62	0.19	0.03	14.59	2.66	0.35	63.92	13.22	3.41
MT02_08	1.11	0.21	0.03	16.90	1.93	0.20	66.22	10.53	2.88
MT02_09	1.72	0.50	0.04	15.96	2.03	0.43	64.14	11.98	3.20
MT02_10	1.13	0.13	0.00	14.08	1.37	0.42	70.54	10.28	2.04
MT04_01	0.69	0.09	0.01	13.99	0.38	0.13	80.61	3.18	0.91
MT04_02	0.72	0.16	0.02	14.13	0.75	0.04	79.27	3.91	1.00
MT04_03	0.82	0.18	0.02	13.51	0.64	0.04	80.87	3.05	0.88
MT04_04	0.76	0.09	0.02	13.13	0.42	0.10	81.63	2.95	0.92
MT04_05	0.76	0.35	0.07	12.06	0.78	0.11	80.89	3.83	1.15
MT04_06	1.42	0.09	0.04	16.36	1.57	0.12	72.97	5.88	1.55
MT04_07	1.41	0.12	0.05	19.24	1.76	0.24	67.26	7.92	2.00
MT04_08	0.82	0.04	0.03	15.26	1.06	0.15	75.38	5.51	1.76
MT04_09	0.85	0.04	0.02	15.14	0.52	0.12	78.07	4.12	1.12
MT04_10	0.95	0.08	0.06	17.35	0.85	0.16	75.46	4.08	1.02
MT05_01	9.00	0.71	0.16	39.99	5.28	0.83	34.44	7.64	1.95
MT05_02	12.55	1.67	0.38	37.06	10.19	1.90	24.15	9.21	2.87
MT05_03	10.63	0.62	0.11	40.11	7.44	1.28	27.25	9.58	2.98
MT05_04	9.38	0.66	0.21	39.64	6.41	1.14	29.17	7.04	6.36
MT05_05	6.98	0.80	0.46	38.31	5.91	1.10	36.39	8.37	1.68
MT05_06	9.67	0.71	0.09	44.52	4.36	0.42	32.76	4.61	2.85
MT05_07	10.22	0.75	0.01	37.23	6.27	0.74	33.89	8.52	2.36
MT05_08	6.66	0.51	0.14	40.06	6.18	0.94	33.63	8.51	3.36
MT05_09	9.20	0.71	0.28	38.28	7.53	0.69	34.19	7.32	1.79
MT05_10	7.63	0.59	0.05	39.72	4.58	0.66	38.02	7.14	1.61
MT06_01	12.11	1.55	0.49	39.64	11.45	1.09	23.39	8.44	1.84
MT06_02	4.39	0.26	0.12	28.03	3.58	0.50	52.29	9.10	1.72
MT06_03	6.69	0.61	0.25	31.51	5.74	0.88	41.21	10.53	2.57
MT06_05	5.91	0.96	0.63	25.73	11.24	1.90	40.30	10.34	2.99
MT06_06	8.02	0.86	0.32	32.95	10.41	1.40	32.70	10.79	2.55
MT06_07	13.08	1.39	0.22	52.45	6.69	0.89	18.26	5.86	1.17
MT06_08	10.04	1.48	0.54	33.33	11.15	1.53	28.99	10.33	2.61
MT06_09	8.27	1.16	0.24	36.33	7.96	1.20	31.56	10.85	2.43
MT06_10	8.24	1.02	0.23	35.15	7.47	1.11	34.28	9.03	3.45
MT07_01	7.62	1.48	0.29	34.97	9.92	1.03	32.45	9.16	3.08
MT07_02	8.75	1.55	0.52	32.12	11.44	1.38	30.33	11.15	2.76
MT07_03	8.64	1.42	0.23	35.97	9.14	1.73	26.78	12.29	3.81
MT07_04	8.29	1.40	0.04	31.19	9.26	1.32	33.69	10.97	3.84
MT07_05	14.65	1.10	0.66	23.41	15.19	0.66	37.71	5.38	1.23
MT07_06	3.27	0.18	0.04	27.70	1.82	0.34	57.51	8.30	0.85
MT07_07	7.17	1.07	0.20	39.69	7.42	1.09	26.97	13.72	2.67
MT07_08	7.87	0.76	0.36	34.86	9.17	1.13	34.08	8.88	2.89

Sample ID	IIIa	IIIb	IIIc	IIa	IIb	IIc	Ia	Ib	Ic
MT07_09	6.34	1.25	0.20	36.96	8.23	0.95	33.91	9.52	2.62
MT07_10	8.93	1.23	0.17	37.81	9.09	1.58	26.82	10.05	4.31
MT08_01	3.36	0.18	0.07	28.89	0.24	0.38	62.95	3.23	0.69
MT08_02	3.82	0.32	0.04	29.39	1.10	0.23	59.59	4.65	0.85
MT08_03	6.30	0.10	0.04	30.63	1.81	0.48	53.23	6.59	0.81
MT08_04	5.39	0.11	0.19	32.86	1.36	0.35	50.91	8.02	0.82
MT08_05	5.73	0.18	0.08	35.86	1.42	0.39	49.30	6.27	0.78
MT08_06	4.30	0.10	0.09	27.29	1.78	0.27	58.45	6.94	0.78
MT08_07	3.86	0.21	0.04	29.61	1.63	0.40	55.84	7.49	0.92
MT08_08	6.29	0.72	0.37	33.89	4.84	1.08	43.48	6.25	3.08
MT08_09	8.33	1.16	0.31	34.02	10.04	1.20	30.49	11.89	2.55
MT08_10	4.91	0.19	0.08	32.35	1.70	0.45	53.63	5.74	0.95
MT09_01	6.11	0.15	0.94	39.92	1.25	1.13	45.60	3.89	1.02
MT09_02	6.12	0.27	0.09	36.50	1.37	0.76	49.27	4.34	1.28
MT09_04	2.29	0.06	0.02	25.31	1.61	0.57	65.14	3.54	1.45
MT09_05	2.94	0.18	0.05	30.45	1.35	0.61	60.27	2.79	1.35
MT09_06	2.73	0.18	0.03	28.60	1.34	0.74	61.04	3.64	1.69
MT09_07	3.59	0.15	0.01	33.04	1.64	0.83	55.58	3.54	1.62
MT09_08	2.86	0.12	0.02	31.82	1.35	0.87	56.76	4.41	1.79
MT09_09	2.75	0.12	0.02	29.67	1.54	0.64	60.18	3.56	1.52
MT09_10	3.12	0.11	0.05	28.48	1.13	0.75	60.88	3.89	1.59
MT12_01	6.41	0.13	0.17	31.50	2.22	0.63	55.67	2.45	0.82
MT12_02	10.23	0.11	0.14	40.77	2.10	0.63	40.62	4.44	0.95
MT12_03	9.84	0.16	0.07	43.67	1.74	0.80	37.93	4.99	0.81
MT12_04	5.88	0.04	0.06	34.93	1.45	0.72	52.77	2.90	1.24
MT12_05	6.36	0.08	0.09	25.62	2.34	0.46	61.59	2.59	0.86
MT12_06	6.59	0.11	0.09	36.55	1.90	1.10	47.63	3.82	2.21
MT12_07	6.93	0.08	0.10	38.29	1.40	0.76	46.37	4.76	1.31
MT12_08	6.09	0.06	0.14	33.35	1.28	0.81	53.25	4.12	0.90
MT12_09	9.29	0.17	0.07	40.09	1.69	1.22	41.99	3.97	1.51
MT12_10	8.29	0.21	0.08	36.52	1.44	0.51	47.75	3.89	1.30
MT13_01	21.05	1.00	0.33	40.64	4.55	1.12	26.32	3.77	1.22
MT13_02	7.57	0.66	0.09	34.71	1.55	0.65	49.99	2.75	2.03
MT13_03	7.93	0.56	0.12	35.55	3.18	0.90	48.12	2.22	1.43
MT13_04	6.29	0.14	0.08	26.54	0.15	0.57	61.28	2.53	2.42
MT13_05	5.25	0.35	0.11	32.02	2.06	0.64	54.32	3.75	1.49
MT13_06	6.53	0.30	0.19	36.07	2.10	0.93	48.70	3.52	1.67
MT13_07	8.24	0.17	0.04	37.75	1.55	0.67	46.99	2.22	2.38
MT13_08	9.50	0.15	0.07	38.15	1.49	0.73	45.55	2.93	1.45
MT13_09	5.87	0.40	0.07	30.64	2.28	0.83	55.75	2.78	1.39
MT13_10	5.23	0.12	0.03	34.66	1.56	1.69	51.56	3.58	1.57
MT14_01	9.97	0.04	0.05	42.30	1.37	0.48	41.62	3.27	0.90
MT14_02	11.86	0.15	0.06	39.91	1.52	0.60	42.71	2.61	0.58
MT14_03	21.43	0.15	0.01	45.87	2.16	0.49	27.45	2.04	0.39
MT14_04	18.81	2.12	0.21	45.17	7.82	0.85	20.57	3.88	0.58
MT14_05	15.87	0.08	0.03	44.47	1.22	0.96	34.34	2.52	0.52
MT14_06	14.04	0.47	0.09	42.62	2.18	0.79	35.84	3.25	0.70
MT14_07	15.81	0.23	0.25	31.34	1.89	0.78	46.87	2.17	0.67

Sample ID	IIIa	IIIb	IIIc	IIa	IIb	IIc	Ia	Ib	Ic
MT14_08	11.10	0.19	0.01	42.49	1.71	0.55	39.21	3.99	0.74
MT14_09	18.72	0.49	0.07	42.14	1.12	0.07	35.54	1.47	0.39
MT14_10	5.57	0.17	0.04	34.63	1.89	0.71	54.20	1.89	0.91
MT15_01	17.90	0.28	0.12	49.25	2.97	0.60	26.82	1.73	0.33
MT15_02	21.75	0.25	0.25	44.59	2.23	0.55	25.66	3.76	0.98
MT15_03	22.14	0.22	0.13	40.05	2.01	0.71	31.29	3.17	0.27
MT15_04	23.62	0.24	0.26	43.59	2.38	3.49	24.74	1.52	0.15
MT15_05	22.13	0.08	0.02	45.11	1.74	0.58	28.03	1.90	0.42
MT15_06	20.16	0.35	0.09	47.60	0.11	0.07	31.49	0.05	0.07
MT15_07	24.36	0.25	0.28	45.46	1.83	0.42	26.57	0.51	0.31
MT15_09	23.45	0.38	0.02	42.91	2.19	2.67	26.65	1.47	0.26
MT15_10	21.20	0.28	0.05	49.60	2.38	0.52	24.48	1.20	0.29
MT16_01	21.06	0.19	0.27	38.97	1.52	0.97	34.58	2.05	0.39
MT16_02	17.04	0.15	0.14	34.95	1.66	1.16	42.21	2.28	0.43
MT16_03	8.81	0.40	0.04	40.18	1.27	0.69	45.64	2.38	0.59
MT16_04	22.08	0.21	0.03	42.44	1.00	0.70	31.89	1.28	0.37
MT16_05	20.86	0.32	0.14	37.28	1.33	1.15	35.37	2.88	0.67
MT16_06	26.76	0.24	0.22	38.47	1.50	0.86	29.84	1.70	0.40
MT16_07	26.43	0.40	0.11	42.06	1.09	0.63	28.05	0.98	0.25
MT16_08	14.84	0.17	0.04	43.49	1.56	1.09	37.96	0.17	0.69
MT16_09	16.97	0.23	0.12	43.10	1.28	0.82	34.48	2.57	0.45
MT16_10	25.26	0.42	0.13	39.18	1.29	0.71	31.80	0.99	0.21
MT17_01	10.29	0.17	0.12	35.09	1.51	0.48	47.23	4.49	0.62
MT17_03	8.56	0.58	0.21	36.92	1.79	0.43	46.76	4.21	0.54
MT17_04	16.31	0.41	0.26	42.01	2.01	0.47	33.80	4.28	0.45
MT17_05	8.61	0.32	0.09	36.72	2.09	0.06	46.74	4.42	0.94
MT17_06	7.95	0.39	0.06	34.90	2.48	0.44	47.61	5.62	0.56
MT17_07	11.79	0.89	0.88	35.97	2.65	1.06	40.86	5.05	0.85
MT17_08	24.78	0.30	0.03	46.81	2.18	0.46	21.77	3.24	0.43
MT17_09	19.04	0.42	0.07	46.28	2.92	0.61	26.98	3.28	0.39
MT17_10	26.15	0.33	0.05	43.71	1.88	0.56	23.97	2.84	0.51
MT18_01	21.25	0.07	0.10	47.76	1.03	0.38	27.60	1.37	0.44
MT18_02	22.63	0.35	0.07	43.89	1.86	0.52	27.03	3.08	0.56
MT18_03	18.85	0.39	0.09	45.05	2.19	0.39	30.55	1.87	0.61
MT18_04	25.73	0.07	0.03	45.64	1.29	0.29	24.63	1.87	0.46
MT18_05	21.92	0.27	0.03	45.90	1.76	0.33	27.83	1.70	0.27
MT18_06	17.22	0.21	0.05	44.70	2.01	0.50	32.02	2.75	0.55
MT18_07	23.33	0.16	0.06	45.44	1.56	0.46	26.68	1.85	0.46
MT18_08	18.56	0.38	0.10	43.65	2.27	0.56	31.08	2.59	0.80
MT18_09	18.11	0.22	0.01	47.26	1.55	0.53	29.87	2.12	0.34